





Characterization of the Protein Tyrosine Phosphatase LmPRL-1 Secreted by *Leishmania major* via the Exosome Pathway

Sabine Leitherer,^a Joachim Clos,^b Elisabeth M. Liebler-Tenorio,^c
Ulrike Schleicher,^{a,d}  Christian Bogdan,^{a,d}  Didier Soulat^{a,d}

Mikrobiologisches Institut-Klinische Mikrobiologie, Immunologie und Hygiene, Universitätsklinikum Erlangen, Friedrich-Alexander-Universität (FAU) Erlangen-Nürnberg, Erlangen, Germany^a; Bernhard Nocht Institute for Tropical Medicine, Hamburg, Germany^b; Institute of Molecular Pathogenesis, Friedrich-Loeffler-Institut, Federal Research Institute for Animal Health, Jena, Germany^c; Medical Immunology Campus Erlangen, FAU Erlangen-Nürnberg, Erlangen, Germany^d

ABSTRACT Similar to other intracellular pathogens, *Leishmania* parasites are known to evade the antimicrobial effector functions of host immune cells. To date, however, only a few virulence factors have been described for *Leishmania major*, one of the causative agents of cutaneous leishmaniasis. Here, we have characterized the expression and function of an *L. major* phosphatase, which we termed LmPRL-1. This enzyme shows a strong structural similarity to the human phosphatases of regenerating liver (PRL-1, -2, and -3) that regulate the proliferation, differentiation, and motility of cells. The biochemical characterization of the *L. major* phosphatase revealed that the enzyme is redox sensitive. When analyzing the subcellular localization of LmPRL-1 in promastigotes, amastigotes, and infected macrophages, we found that the phosphatase was predominantly expressed and secreted by promastigotes via the exosome route. Finally, we observed that ectopic expression of LmPRL-1 in *L. major* led to an increased number of parasites in macrophages. From these data, we conclude that the *L. major* phosphatase LmPRL-1 contributes to the intracellular survival of the parasites in macrophages.

KEYWORDS *Leishmania*, exosome, macrophage, tyrosine phosphatase

Leishmaniasis is an infectious disease prevalent worldwide that is caused by kinetoplastid protozoan parasites belonging to the genus *Leishmania* (1). In nature, this heteroxenous parasite is transmitted by the bites of sand flies. Following the inoculation of flagellated promastigotes into the dermis of the host, the parasites are rapidly endocytosed by phagocytic cells, in which they differentiate into amastigotes, multiply, and reach inner compartments and organs, such as draining lymph nodes, spleen, liver, and bone marrow. The life cycle of the parasite is completed after ingestion of amastigote-infected cells by sand flies during their blood meal. In the digestive tract of their vector, parasites transform back into extracellular promastigotes that develop into infectious metacyclics (2). Depending on the status of the host immune system and the *Leishmania* species, the infection of mammals leads either to mostly self-healing skin lesions (cutaneous leishmaniasis [CL]) or to a systemic disease, termed visceral leishmaniasis (VL) or kala-azar, that is lethal if untreated (3–5).

To survive in their hosts, *Leishmania* parasites need to quickly adapt their growth, metabolism, and mechanisms of protection to their new environment. Interestingly, only a few genes are differentially expressed during this adaptive process, suggesting an important role for the regulation of protein translation (6). *Leishmania* species-specific gene diversity also participates in the adaptation of the parasite to its organ-

Received 6 February 2017 Returned for
modification 28 February 2017 Accepted 11
May 2017

Accepted manuscript posted online 15 May
2017

Citation Leitherer S, Clos J, Liebler-Tenorio EM,
Schleicher U, Bogdan C, Soulat D. 2017.
Characterization of the protein tyrosine
phosphatase LmPRL-1 secreted by *Leishmania
major* via the exosome pathway. Infect Immun
85:e00084-17. <https://doi.org/10.1128/IAI.00084-17>.

Editor John H. Adams, University of South
Florida

Copyright © 2017 American Society for
Microbiology. All Rights Reserved.

Address correspondence to Didier Soulat,
didier.soulat@uk-erlangen.de.

specific microenvironment in the host (7). The stress response protein A2 is an example of such a gene, expressed only by *Leishmania* species causing VL. A2 appears to mediate heat shock resistance and thereby to support parasite survival and visceralization in inner and warmer organs (8). Other *Leishmania* genes were found to regulate the promastigote-to-amastigote transformation and the intracellular growth of amastigotes; examples include the genes encoding the cation transporter-like protein MGT2 (9), the MPK7 protein kinase (10), and the homologue of the proliferation-associated 2G4 protein Ebp1, named LmaPA2G4 (11).

In addition to these adaptive responses, *Leishmania* parasites have also developed strategies to manipulate the phagocytic cells in which they primarily reside (reviewed in references 12–16). Recent studies revealed that homologues of the macrophage migratory inhibitory factor expressed by *Leishmania major*, LmMIF-1 and -2, can alter the leishmanicidal activity of macrophages, leading to T cell exhaustion and disease progression during *in vivo* infection (17, 18). Similarly, another well-studied immunomodulatory molecule of *Leishmania* is its promastigote surface molecule lipophosphoglycan (LPG) (19, 20), which delays the fusion of the phagosome with late endosomes or lysosomes in macrophages (21, 22). In addition, parasites secrete virulence factors, such as the zinc metalloprotease Gp63 (also known as leishmanolysin) or the elongation factor EF-1 α , to inhibit the production of leishmanicidal nitric oxide or of proinflammatory cytokines by macrophages (15, 23, 24). These two parasite-derived factors lead to the rapid activation of src homology 2 domain-containing tyrosine phosphatase 1 (SHP-1) and other host phosphatases (25, 26), the modulation of protein kinase C (PKC) activities (27, 28), the inhibition of mitogen-activated protein kinase (MAPK) (29, 30), and the disruption of the Janus kinase (JAK)/signal transducer and activator of transcription (STAT) pathway after *Leishmania* infection (14, 25, 31). Altogether, the changes in host kinase and phosphatase activity caused by these virulence factors contribute to the immune silencing induced by *Leishmania*.

Although these host cellular pathways all rely on phosphorylation events, so far no *Leishmania* virulence factor has been reported to directly modulate the phosphorylation status of host proteins (32, 33). Despite the presence of secreted or membrane-bound acid phosphatases in different *Leishmania* species, such as histidine acid phosphatases (34–36), there is only limited evidence to support a function of these enzymes in the virulence of the parasite (37–39). Moreover, to date, neither their mechanisms of action nor their modes of access to the host cell cytoplasm have been elucidated.

In our present study, we focused on *L. major*, one of the causative agents of CL, which is prevalent in the Near and Middle East, northern Africa, the northwestern states of India, and presumably also in northwestern China (40, 41). Here, we identify a new tyrosine phosphatase encoded by *L. major*. First, we characterize the biochemical activity of this *Leishmania* phosphatase, which we named LmPRL-1 due to its similarity to the family of mammalian phosphatases of the regenerating liver (PRLs). PRLs are thought to participate in the control of various cellular processes, such as proliferation, differentiation, and motility (42). Second, we provide evidence that the LmPRL-1 phosphatase can be secreted during infection of macrophages and that it contributes to the survival of the parasite in these host cells.

RESULTS

The *Leishmania* phosphatase LmPRL-1 is a homologue of the human PRLs. Our research on new virulence factors of *L. major* focuses on proteins that are putatively released by parasites and that might affect the host cell signaling machinery. *Leishmania* parasites secrete proteins mainly via exosomes. The analysis of the protein content of these exosomes (43, 44) combined with the genome analysis (data not shown) of our *L. major* strain (MHOM/IL/81/FEBNI) (45) allowed us to identify a gene on chromosome 16 ([LmjF.16.0230](#)) that is identical to the one annotated in the *L. major* Friedlin strain (46) and encodes a protein tyrosine phosphatase (PTP) here called LmPRL-1. A BLAST search with this gene revealed the presence of a paralogous gene ([LmjF.16.0250](#)) on the same chromosome 16 of *L. major*. However, the protein product of this gene (which we

termed LmPRL-2) was not reported in the published exosome analyses (43, 44), excluding the enzyme from the list of putative new secreted virulence factors. In addition, the BLAST results revealed that LmPRL-1 belongs to the PRL family (Fig. 1A and B) and that there are numerous homologues in the family *Trypanosomatidae*.

The phylogenetic analysis of all available sequences of *Trypanosomatidae* that are homologues of mammalian PRL sequences uncovered a peculiar gene organization for the genus *Leishmania*. All 17 sequenced species of *Leishmania* except *L. panamensis* include two PRL-related phosphatases in their genomes, as seen in *L. major* (strain Friedlin). Moreover, these paralogous genes always segregate separately in the phylogenetic tree, creating two subfamilies of genes, one related to *LmjF.16.0230* (Fig. 1A, blue branch) and the other related to *LmjF.16.0250* (Fig. 1A, green branch). Interestingly, this pairwise organization has also been observed in the genera *Leptomonas*, *Endotrypanum*, and *Crithidia*, whereas the gene number can vary from one to four copies in the genus *Trypanosoma* (Fig. 1A). Our overall knowledge about this phosphatase family in *Trypanosomatidae* is still very limited. So far, only one study has reported the expression of a family member, termed TcPRL-1. This protein, which is encoded by the gene *TcCLB.503851.24* (Fig. 1A, arrow), was detected in amastigote extracts of *Trypanosoma cruzi*, but its function has not yet been studied (47). A high-throughput RNA interference (RNAi) screen performed in *Trypanosoma brucei* led to the discovery of the gene *Tb927.8.5780* (Fig. 1A, arrowhead), which might be involved in the survival of the parasite during *in vitro* differentiation (48). However, one has to be cautious with extrapolations, as *T. cruzi* has four paralogues of PRL-like genes whereas *T. brucei* carries only one.

The two *L. major* phosphatases, LmPRL-1 and LmPRL-2, show 58.5% identity, 26.2% similarity, and only a 15.3% difference in their amino acid sequences. The LmPRL-1 and LmPRL-2 proteins also share strong sequence identity (between 38.9 and 41.1%) with the three proteins of the human PRL phosphatase family (PRL-1, -2, and -3) (Fig. 1B), which themselves form a homogeneous group of proteins with a high degree (>75%) of amino acid sequence identity (Fig. 1B). This strong protein sequence relationship translates into comparable structural organizations, as shown by the alignment of the human PRL-1 crystal structure (Protein Data Bank [PDB] no. 1XM2) (49) with the crystal structure of *L. major* LmPRL-1 (PDB no. 3S4O) (Fig. 1C). The structures of both proteins consist of α -helices surrounding a five-stranded β -sheet, which represents the canonical structure of tyrosine phosphatases. This alignment also illustrates the highly conserved orientation of the amino acids that are critical for their phosphatase activity (Fig. 1C). The P loop and the WDP loop are maintained in all mammalian PRL and *Leishmania* PRL-like sequences (Fig. 1D). Interestingly, the catalytic cysteine 114 located in the C-X₅-R P loop of LmPRL-1 (C107 for LmPRL-2) neighbors cysteine 53 in loop 2 (C52 for LmPRL-2) (Fig. 1C). In PRL-1, this proximity between cysteines was previously described as essential for the regulation of catalytic activity, since the two residues could form an inactivating disulfide bond (50, 51). Another important feature shared by all these phosphatases is the presence of a farnesylation site (C-A-A-X) at the C terminus of the protein, which suggests possible membrane localization for the *Leishmania* phosphatases (Fig. 1B). Membrane localization is also supported by the interaction between a nearby polybasic sequence (Fig. 1B) and the negatively charged phospholipids present in the cellular membrane (52).

Despite all these similarities between mammalian and *Leishmania* PRLs, substantial differences can be observed in the sequences of loops 1 and 2 that are crucial to the substrate specificity of a PTP. As illustrated in Fig. 1D, LmPRL proteins share only 2 out of 9 amino acid residues with loop 1 of mammalian PRL, namely, proline 29/28 (LmPRL-1/2) and leucine 34/33. Regarding loop 2, the divergence is also remarkable, as only 4 out of 7 residues are conserved, namely, arginine 51/50, cysteine 53/52, threonine 56/55, and tyrosine 57/56. Interestingly, there are also differences in the sequences of the two loops in the different *Leishmania* PRL-like proteins (Fig. 1D). Asparagine 33 of loop 1 of LmPRL-1 is replaced by serine 32 in LmPRL-2. Similarly, valine 52 of loop 2 of LmPRL-1 is replaced by alanine 51 in LmPRL-2. These differences

discriminate between the LmPRL-1 like and LmPRL-2 like proteins described in the phylogenetic tree. Altogether, these amino acid sequence disparities suggest a distinct substrate specificity of *Leishmania* and human PRLs.

Characterization of the enzymatic activity of recombinant His₆-LmPRL-1. As the protein LmPRL-1 was the only PTP detected in *Leishmania* exosomes (43, 44), we focused our further investigation on that enzyme. To assess their enzymatic functions, the *Leishmania* protein LmPRL-1 and the human PRL-1 were overexpressed in *E. coli* cells with a His₆ tag and purified by affinity chromatography using a Ni-nitrilotriacetic acid (NTA) matrix. Hydrolysis of *para*-nitrophenyl phosphate (pNPP), a classical PTP substrate, was monitored to determine their enzymatic activities. Despite purification under reducing conditions (5 mM β-mercaptoethanol), hydrolysis was hardly detectable unless the enzymes were preincubated with 10 mM dithiothreitol (DTT) for 1 h (Fig. 2A). Under both nonreducing and reducing conditions, the activities detected for His₆-LmPRL-1 were in the same order of magnitude as those measured for the human His₆-PRL-1 (Fig. 2A). Since PRL-1 has higher affinity for the fluorogenic substrate 6,8-difluoro-4-methylumbelliferyl phosphate (DiFMUP), this substrate was chosen for the further catalytic study of His₆-LmPRL-1 (50). The optimal pH for the activity of His₆-LmPRL-1 turned out to be slightly acidic (pH 6.0) (Fig. 2B). In addition, the kinetic characteristics of the *Leishmania* phosphatase were determined. A V_{max} of 2.6×10^{-5} M/min/g and a K_m of 9.32×10^{-6} M were measured for the dephosphorylation of DiFMUP. Considering the requirement for a reducing milieu, we also investigated the roles of the putative catalytic and regulatory cysteines. First, the activity of a serine mutant of the catalytic cysteine C114 was tested. As expected, the phosphatase activity of the His₆-LmPRL-1-C114S mutant was fully abolished (Fig. 2C). In contrast, a mutant of the putative regulatory cysteine, His₆-LmPRL-1-C53S, showed markedly higher activity toward DiFMUP (>2-fold increase compared to wild-type [WT] enzyme) (Fig. 2C). The latter finding suggested that a disulfide bond formed between the regulatory and the catalytic cysteine needs to be reduced to trigger the LmPRL-1 phosphatase activity. To further validate this hypothesis, the migration behaviors of the WT protein and the different mutants of the His₆-tagged phosphatase were analyzed with nonreducing SDS-PAGE, as it allows the indirect visualization of disulfide bond formation. Under oxidative conditions, a protein containing an oxidized disulfide bond runs at a lower molecular weight than predicted because the sequence is more compact (53). The WT phosphatase, pretreated with 10 mM oxidized DTT, migrated as two bands. The predominant lower band corresponds to the oxidized form, whereas the minor upper band corresponds to the reduced form of His₆-LmPRL-1 (Fig. 2D). Only the latter form was detectable when the protein was preincubated with 10 mM reduced DTT, leading to the reduction of the disulfide bond. Similar treatment of mutants of either the catalytic (His₆-LmPRL-1-C114S) or the regulatory (His₆-LmPRL-1-C53S) cysteine revealed that these proteins could no longer convert into an oxidized, fast-migrating form. These data support a regulatory mechanism for the phosphatase activity of LmPRL-1 based on a pair of cysteines that sense the redox potential of the milieu.

FIG 1 Homology between *L. major* phosphatases, LmPRL-1 and LmPRL-2, and their homologues from the PRL family in mammals and *Trypanosomatidae*. (A) Phylogenetic comparison between the mammalian PRLs and their homologues in *Trypanosomatidae*. Available gene sequences belonging to the PRL family from all *Trypanosomatidae* and from mouse and human, were used to construct a phylogenetic topology by the minimum-evolution method. The circles indicate nodes supported in ≥70% (open), ≥80% (gray), or ≥90% (black) of 500 random bootstrap replicates of all neighbor-joining trees. The evolutionary distance (scale) is measured in numbers of base substitutions per site. Sequences are labeled in red for mammalian, black for *Leishmania*, cyan for *Endotrypanum*, violet for *Crithidia*, pink for *Leptomonas*, and orange for *Trypanosoma*. The red stars indicate LmPRL-1 (LmjF.16.0230) and LmPRL-2 (LmjF.16.0250). (B) Comparison of LmPRL-1 (Q4QEZ7) and LmPRL-2 (Q4QEZ5) protein sequences with those of the three members of the phosphatase of the regenerating liver family, PRL-1 (Q93096), PRL-2 (Q12974), and PRL-3 (O75365) (the references in parentheses refer to the UniProtKB database). The CLUSTAL W program (86) was used for the alignment. The asterisks indicate amino acid residues identical in all proteins, and the colons indicate similarity. The catalytic cysteine is indicated in red and the regulatory cysteine in orange. The different loops involved in the catalytic site, the polybasic region, and the putative farnesylation site are indicated with black lines. (C) Alignment of the three-dimensional (3D) structures of LmPRL-1 (PDB no. 3S4O) (blue) and PRL-1 (PDB no. 1XM2) (gray). PyMOL software was used to align the proteins, represented in cartoon form. The vicinity of the catalytic cysteines of LmPRL-1 and PRL-1, C114 and C104, respectively, is illustrated in the box, revealing their close proximity to the regulatory cysteines of the two proteins C53 and C49, respectively. (D) Conservation of loop sequences. The sequences of the conserved amino acids of the four loops described in panel B are listed for the mammalian PRLs (PRL group; red branch in panel A), the LmPRL-1-like phosphatases of *Leishmania* (panel A, blue branch), and the LmPRL-2-like phosphatases of *Leishmania* (panel A, green branch).

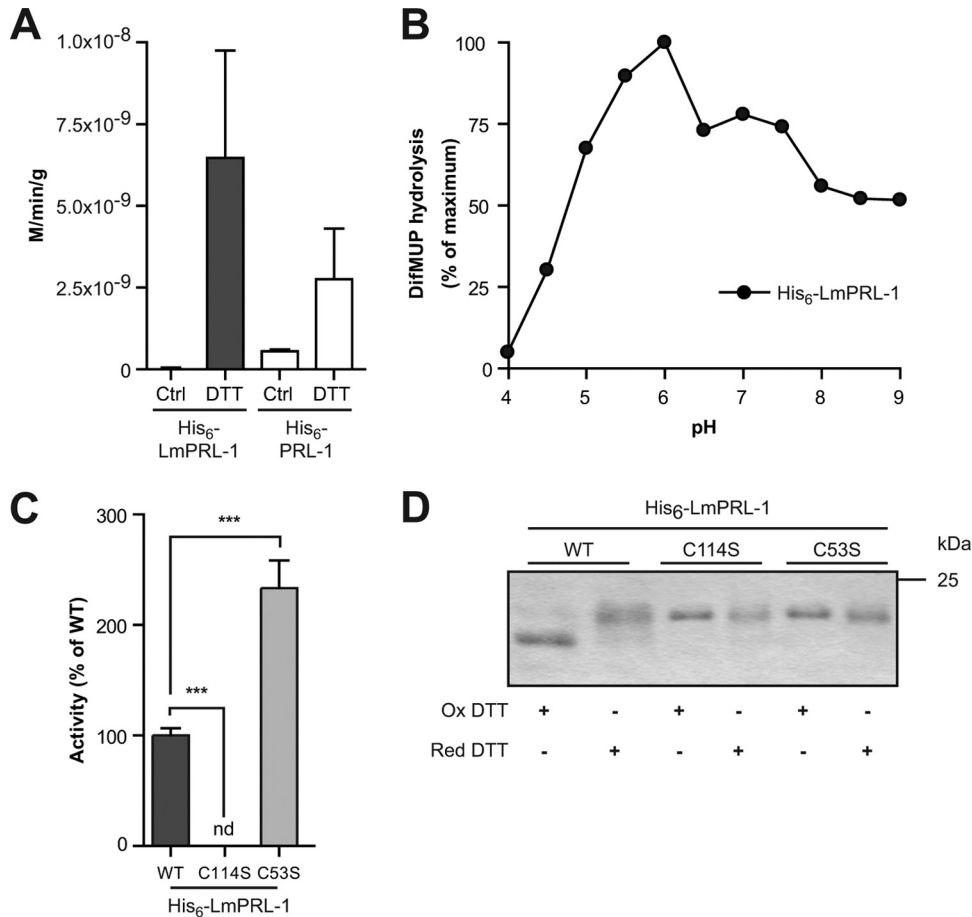


FIG 2 Biochemical characterization of His₆-tagged LmPRL-1. (A) Phosphatase activity of WT His₆-LmPRL-1 against pNPP compared to the activity of the human His₆-PRL-1. The phosphatase activity was measured by incubating His₆-tagged LmPRL-1 (black bars) and PRL-1 (white bars) with pNPP for 1 h at 37°C and pH 6.0. Some reactions were carried out with previously reduced proteins. (B) Phosphatase activity of WT His₆-LmPRL-1 against DiFMUP as a function of pH. His₆-tagged LmPRL-1 was reduced before its phosphatase activity was measured by incubating it with DiFMUP for 20 min at 37°C and pHs varying from 4.0 to 9.0. (C) Effects of the catalytic (C114) and regulatory (C53) cysteines on the phosphatase activity of His₆-LmPRL-1. The phosphatase activities of His₆-LmPRL-1-C114S and His₆-LmPRL-1-C53S (light-gray bar) against DiFMUP at pH 6.0 after 20 min at 37°C were measured and compared to the activity of the wild-type His₆-LmPRL-1 (dark-gray bar). (D) Change of the electrophoretic migration of LmPRL-1 induced by oxidation is controlled by the catalytic and regulatory cysteines. The wild type and the catalytic and regulatory mutants of LmPRL-1 were either oxidized with 10 mM oxidized (Ox) DTT or reduced with 10 mM reducing (Red) DTT for 1 h at 4°C. The proteins were separated on nonreducing SDS-PAGE and dyed by Coomassie staining. The data represent the means and SD of the results of one of three experiments with similar results. ***, *P* < 0.001; nd, not determined.

LmPRL-1 expression and subcellular localization in *L. major* promastigotes and amastigotes.

As an initial step toward its functional characterization, we investigated whether the LmPRL-1 phosphatase shows a parasite stage-dependent expression pattern. To this end, we obtained a rabbit anti-LmPRL-1 peptide antiserum and generated *L. major* parasites that ectopically expressed hemagglutinin (HA₃)-tagged LmPRL-1 (23.1 kDa) following electroporation of pCLN-3xHA-based vectors (see Table S1 in the supplemental material). As a control, we also expressed HA₃-LmPRL-2 in *L. major* to ascertain the specificity of the rabbit anti-LmPRL-1 antiserum and to exclude the detection of this paralogous protein. Western blot analysis of lysates of these parasites revealed that both HA-tagged proteins could be expressed (Fig. 3A, α-HA) and that the anti-LmPRL-1 antiserum selectively detected HA₃-LmPRL-1 (Fig. 3A, α-LmPRL-1, arrow); no cross-reaction with HA₃-LmPRL-2 was observed. Furthermore, endogenous LmPRL-1 (19.4 kDa) was detectable in the lysates of the two strains ectopically expressing HA₃-tagged proteins, as well as in the lysate of the WT *L. major* strain (Fig. 3A, α-LmPRL-1, asterisk).

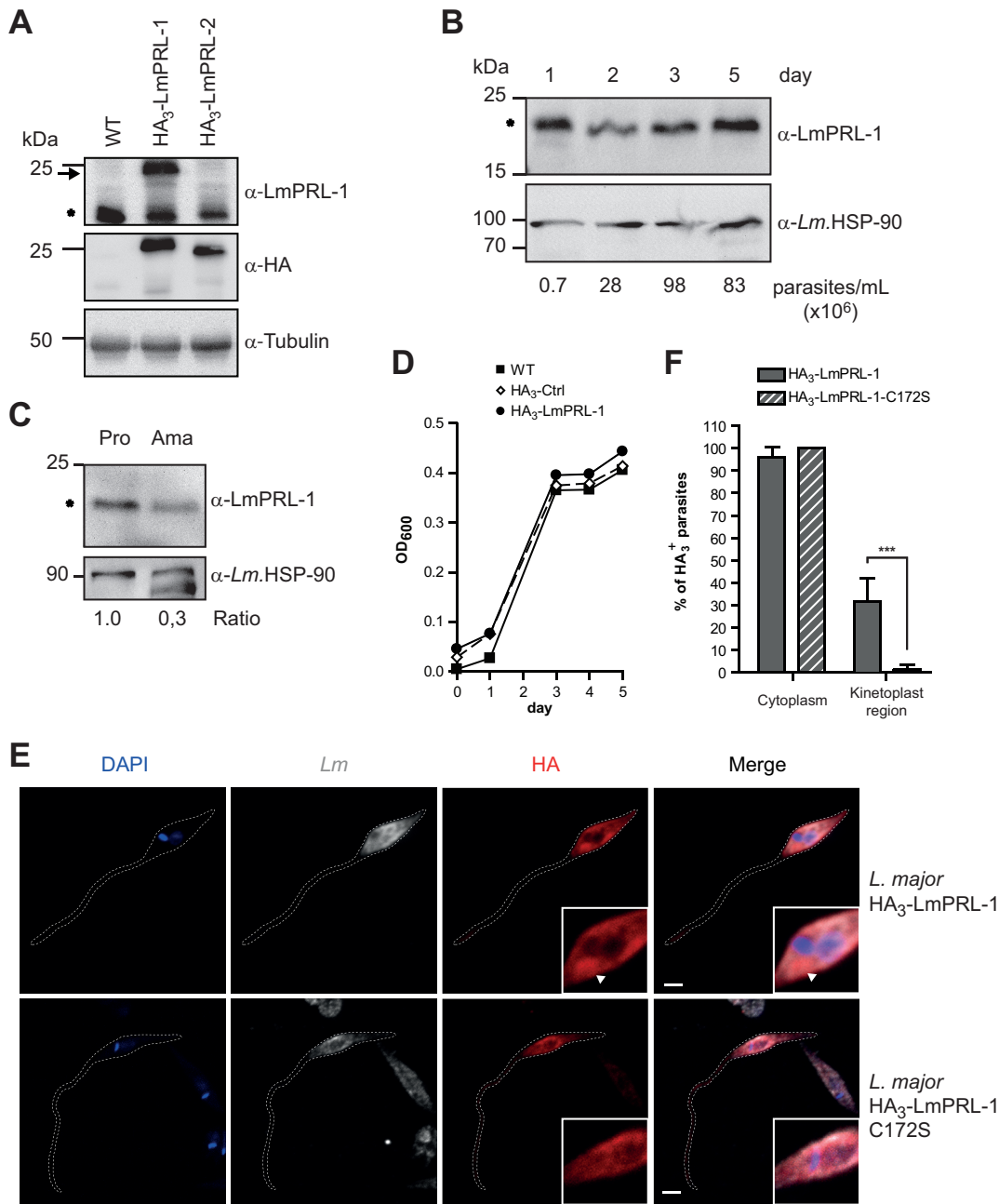


FIG 3 Expression and subcellular localization of LmPRL-1 in *L. major* parasites. (A) Detection of LmPRL-1 protein in promastigotes. Protein extracts were prepared from stationary-phase promastigote cultures of WT *L. major* and parasites ectopically expressing HA₃-LmPRL-1 or HA₃-LmPRL-2. The proteins were analyzed by immunoblotting with rabbit serum anti-LmPRL-1, as well as anti-HA antibody to estimate the specificity of the rabbit serum and with anti-tubulin antibody (loading control). Endogenous LmPRL-1 (expressed by WT parasites) is indicated by the asterisk and HA₃-tagged proteins of transfected *L. major* by the arrow. (B) Expression of LmPRL-1 in logarithmic- or stationary-growth-phase promastigotes *in vitro*. A culture of WT *L. major* promastigotes in modified complete Schneider's medium inoculated with 1.0×10^5 parasites/ml was analyzed daily for its concentration (parasites per milliliter) until it reached stationary phase (day 5). Expression of endogenous LmPRL-1 (marked by the asterisk) was analyzed by anti-LmPRL-1 immunoblotting, using the HSP-90 housekeeping gene as a control. (C) Expression of LmPRL-1 in promastigotes and amastigotes. Protein extracts prepared from the same number (20×10^6) of *in vitro*-cultivated promastigotes (Pro) and *ex vivo*-isolated amastigotes (Ama) were loaded onto SDS-PAGE. Expression of endogenous LmPRL-1 (marked by the asterisk) and of the HSP-90 housekeeping gene was analyzed by immunoblotting. The ratios of the band intensities are indicated below. (D) Ectopic expression of HA₃-LmPRL-1 has no effect on *in vitro* growth of *L. major* promastigotes. WT promastigotes and parasites either carrying the empty pCLN-3xHA vector or expressing HA₃-LmPRL-1 were cultivated in modified complete Schneider's medium starting at 1.0×10^5 parasite/ml until stationary phase. Growth was monitored by measuring the OD₆₀₀. (E and F) Subcellular localization of LmPRL-1 in *L. major* promastigotes depends on its C-terminal farnesylation. (E) Parasites expressing HA₃-LmPRL-1 or HA₃-LmPRL-1-C172S were analyzed by confocal microscopy after staining with an anti-HA antibody (red), an anti-*Leishmania* serum (gray), and DAPI (blue). The arrowheads indicate the region of the kinetoplast. Bars, 2 μ m. (F) Means and standard deviations of more than 250 promastigotes per strain of *L. major*. ***, $P < 0.001$. The data presented are from one of three experiments with similar results.

Next, we tested whether the flagellated promastigote form of *L. major* parasites expressed different amounts of LmPRL-1 depending on the growth phase. In their logarithmic growth phase (days 1 to 3 of culture), promastigotes were clearly positive for LmPRL-1 (Fig. 3B, asterisk). The stationary-phase promastigotes (day 5 of culture), which represent the more infectious stage of the parasite, maintained the expression of LmPRL-1 (Fig. 3B). When analyzing the expression of the phosphatase in 20×10^6 amastigotes prepared from the skin lesions of infected BALB/c mice, we found that LmPRL-1 was still expressed in this developmental stage but to a considerably lesser extent per cell than in the same number of stationary-phase promastigotes (Fig. 3C, asterisk).

To characterize the localization and fate of LmPRL-1 inside *Leishmania* parasites, rabbit anti-LmPRL-1 serum was tested on WT *L. major* promastigotes. Unfortunately, the quality of the rabbit anti-LmPRL-1 serum was not sufficient for reliable detection of LmPRL-1 by confocal laser scanning fluorescence microscopy (CLSM). Therefore, we used parasites ectopically expressing the HA₃-tagged protein. During a culture period of 5 days, the growth rates of the HA₃-LmPRL-1-expressing promastigotes of the WT parent strain and of a parasite line carrying the empty HA vector (HA₃-Ctrl) were comparable (Fig. 3D). The subcellular localization of HA₃-LmPRL-1 was analyzed by CLSM. The cytosol of more than 97% of the promastigotes analyzed stained positively for HA₃-LmPRL-1 (Fig. 3E and F). In addition, the protein appeared to be enriched around the kinetoplast in 30% of the parasites (Fig. 3F). Strikingly, the accumulation of HA₃-LmPRL-1 in the kinetoplast region was dependent on its C-terminal farnesylation motif. As illustrated in Fig. 3E and F, the C172S mutation of the C-A-A-X sequence resulted in diffuse cytosolic staining and loss of staining around the kinetoplasts of the parasites. This result demonstrates that the farnesylation motif of LmPRL-1 is functional in *L. major* promastigotes. Since the kinetoplast region is in close proximity to the flagellar pocket in promastigotes, which has been described as a region actively involved in protein secretion and in the production of exosomes (54, 55), these data are indicative of secretion of the LmPRL-1 phosphatase by *Leishmania* parasites during infection.

LmPRL-1 is secreted by *L. major* promastigotes via the exosome pathway. To validate the possible association of LmPRL-1 with exosomes of *L. major*, exosomes from a culture of WT stationary-phase promastigotes were purified by ultracentrifugation following established protocols (43). Using electron microscopy, a homogeneous population of vesicles with sizes ranging from 70 to 150 nm was observed, confirming that the integrity of the exosomes was maintained during purification (Fig. 4A). The protein content of these exosomes was analyzed by Western blotting. LmPRL-1, as well as HSP70, a protein enriched in *Leishmania* exosomes (56), was detected in the exosome preparation (Fig. 4B, top, left lane). In addition, the purified exosomes were subjected to trypsin digestion. LmPRL-1 was not degraded by trypsin alone (Fig. 4B, top, middle lane), whereas in the presence of the detergent Triton X-100, both the LmPRL-1 band and the HSP70 protein disappeared (Fig. 4B, top, right lane). This indicates that LmPRL-1 and the known exosome marker HSP70 were protected from the action of the protease by the exosome phospholipid membrane. Similar results were obtained with exosomes produced by parasites expressing HA-tagged WT LmPRL-1, indicating that this N-terminal tag does not impair the release of the phosphatase in exosomes (Fig. 4C). Surprisingly, HA-tagged LmPRL-1 with a mutated farnesylation motif (HA₃-LmPRL-1-C172S) was also detected inside exosomes (Fig. 4D), suggesting that the loading of exosomes with LmPRL-1 does not require a functional farnesylation site. Finally, to exclude direct secretion of the phosphatase by the parasite through the classical secretory pathway, we also estimated the quantity of LmPRL-1 secreted outside exosomes. The protein content of the supernatants (SN) resulting from the ultracentrifugation step during the preparation of *L. major* exosomes was precipitated and analyzed by Western blotting. The majority of LmPRL-1 was detected in the pelleted exosomes, whereas only a minor proportion of the protein was found in the soluble supernatants

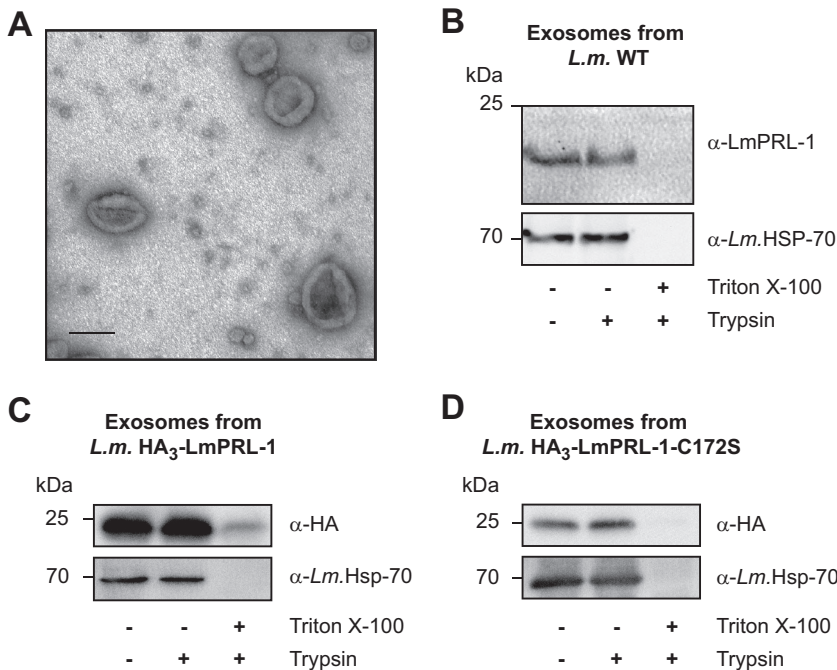


FIG 4 LmPRL-1 is secreted by *L. major* promastigotes via exosomes. (A) Electron micrograph of exosomes produced by WT *L. major* promastigotes. Exosomes were purified from a culture of metacyclic promastigotes incubated overnight in serum-free RPMI 1640 medium at 28°C and then fixed and analyzed by electron microscopy. Bar, 100 nm. (B) Endogenous LmPRL-1 is secreted in exosomes of WT *L. major* (*L.m.*) promastigotes. Purified exosomes from WT promastigotes were analyzed by immunoblotting for the presence of LmPRL-1 and the exosome marker HSP-70. Untreated exosomes were compared to exosomes digested with trypsin or with trypsin in the presence of the detergent Triton X-100. (C) Ectopic expression and HA tagging does not alter LmPRL-1 secretion via exosomes. Purified exosomes from transfected *L. major* ectopically expressing HA₃-LmPRL-1 were analyzed by immunoblotting for the presence of HA-tagged protein and the exosome marker HSP-70 following treatment similar to that described for panel B. (D) HA-tagged LmPRL-1 is secreted in exosomes independently of its farnesylation motif. Purified exosomes from transfected *L. major* ectopically expressing HA₃-LmPRL-1-C172S were analyzed as described for panel C. The data presented are from one of three experiments with similar results.

(see Fig. S1 in the supplemental material). Overall, these results clearly show that WT or HA-tagged LmPRL-1 is secreted by *L. major* promastigotes inside exosomes.

LmPRL-1 is expressed during macrophage infection by *L. major* promastigotes.

Having established that LmPRL-1 can be secreted by *L. major* promastigotes, its expression and fate during infection of macrophages were analyzed. Bone marrow-derived macrophages (BMM) were infected with WT stationary-phase *L. major* promastigotes at a multiplicity of infection (MOI) of 5. The infection was ascertained by the specific detection of the *L. major* HSP90 protein. Increasing amounts of HSP90 were detected during the course of the experiment (Fig. 5). The slight decrease in HSP90 observed after 72 h of infection reflects the reduced number of intracellular parasites due to spontaneous killing by BMM. LmPRL-1 was clearly present in the lysates of promastigote-infected BMM throughout the *in vitro* infection (Fig. 5, asterisk). We also directly infected BMM with amastigotes purified from skin lesions of infected and nonhealing BALB/c mice. Unexpectedly, LmPRL-1 was hardly detectable in amastigote-infected BMM throughout the observation period (Fig. 5). These data show that LmPRL-1 is present in promastigote-infected macrophages for at least 72 h but remains downregulated in lesional amastigotes even after *in vitro* uptake by cultured macrophages.

HA₃-LmPRL-1 is secreted by *L. major* during macrophage infection. To follow the fate of *Leishmania* LmPRL-1 after infection, BMM were infected with *L. major* promastigotes expressing the HA₃-tagged phosphatase. After 72 h of infection, the subcellular localization of the proteins was analyzed by CLSFM. Whereas no HA-derived

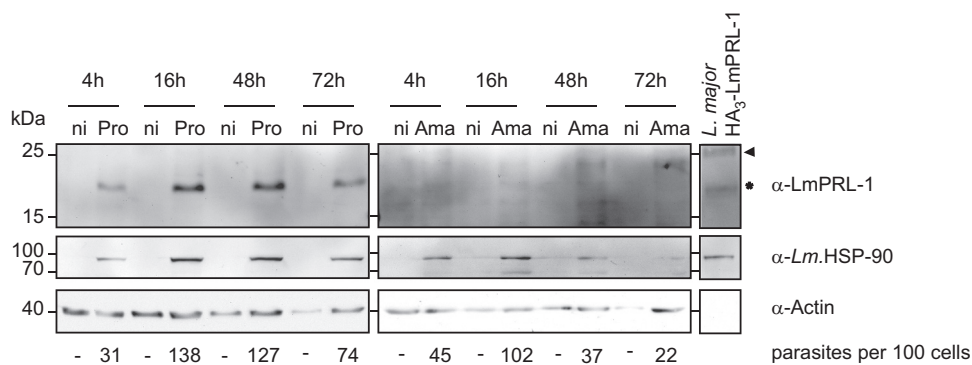


FIG 5 Expression of LmPRL-1 during macrophage infection by *L. major*. BMM were infected by *L. major* WT promastigotes (Pro) or amastigotes (Ama) at an MOI of 5. Noninfected BMM (ni) were used as controls. At the indicated time points, protein samples were analyzed by immunoblotting for the expression of LmPRL-1, *Leishmania* HSP-90, and BMM actin. Lysates of parasites ectopically expressing HA₃-LmPRL-1 were used to control the reactivity of the LmPRL-1 antiserum. WT LmPRL-1 protein is marked with an asterisk and HA₃-LmPRL-1 with an arrowhead. The numbers of parasites per 100 cells of the culture are shown below the Western blots. BMM were infected with *L. major* promastigotes or amastigotes at an MOI of 5. Extracellular parasites were washed away with PBS (2×) after 4 or 16 h. At the indicated time points, Diff-Quik staining was performed, and the number of amastigotes per 100 cells was determined (a total of 300 cells/per sample). The data presented are from one of three experiments with similar results.

staining was seen in BMM infected with *L. major* carrying the empty control vector pCLN-3xHA (Fig. 6A, c), *L. major* parasites expressing HA₃-tagged LmPRL-1 were readily detectable as amastigotes (Fig. 6A, e to h) inside parasitophorous vacuoles (PV) that were labeled by an antibody (Ab) against the lysosome-associated membrane protein 1 (LAMP-1) (Fig. 6A, f, arrowheads). In addition, a HA signal was also consistently detected outside the PV when the macrophages were infected with HA₃-LmPRL-1 parasites (Fig. 6A, g, thin arrows), whereas no signal was detected in noninfected cells (Fig. 6A, g, thick arrows). This distribution pattern indicates that HA₃-LmPRL-1 leaves the PV and enters the cytoplasm of host cells, which is in line with the detected exosome-dependent secretion of LmPRL-1 by WT *Leishmania* (Fig. 4).

A closer microscopic analysis of macrophages infected with *L. major* expressing HA₃-LmPRL-1 confirmed its diffuse intraparasitic localization and its presence outside the PV (Fig. 6B, g, thin arrow). We also observed LAMP-1-positive compartments that were decorated with HA₃-LmPRL-1 and contained amastigote parasites (Fig. 6B, e to h, arrowheads). To confirm the secretion of HA₃-LmPRL-1 during macrophage infection, subcellular fractions were prepared from BMM infected with either HA₃-Ctrl or HA₃-LmPRL-1 for 72 h. Most of the HA signal was detected in the heaviest fraction pelleted at 3,000 × *g* (Fig. 6C, P3). This fraction comprises the BMM nuclei and large organelles, such as PV containing amastigotes that express the HA₃-tagged protein. The latter account for the presence of *Leishmania* HSP90, *Leishmania* tubulin, and the phagolysosome marker LAMP-1. LAMP-1, but not tubulin or HSP90, was also detected in the P100 fraction containing small vesicular structures and the cytoplasmic membrane. HA₃-LmPRL-1 was probably detected in this fraction because of the destruction of some PV vacuoles (Fig. 6C, P100). Strikingly, HA₃-LmPRL-1 was also detected in the cytosolic fractions of infected cells (Fig. 6C, S100), in which only tubulin and *Leishmania* HSP90, but no LAMP-1, were found. Altogether, these data document the fate of HA₃-LmPRL-1, which is first secreted by *Leishmania* parasites during infection and then appears to reach the cytoplasm of infected cells.

HA₃-LmPRL-1 expression by *L. major* increases parasite survival during infection of macrophages. Finally, we tested the effect of HA₃-LmPRL-1 overexpression on the intracellular survival of *L. major*. BMM were infected at an MOI of 5 for 16, 48, or 72 h with either the control strain of *L. major* (HA₃-Ctrl) or the strain ectopically expressing HA₃-LmPRL-1. For each time point, the number of intracellular parasites per 100 macrophages of the culture was calculated by measuring the infection rate and determining the number of parasites per infected macrophage. After 72 h of infection,

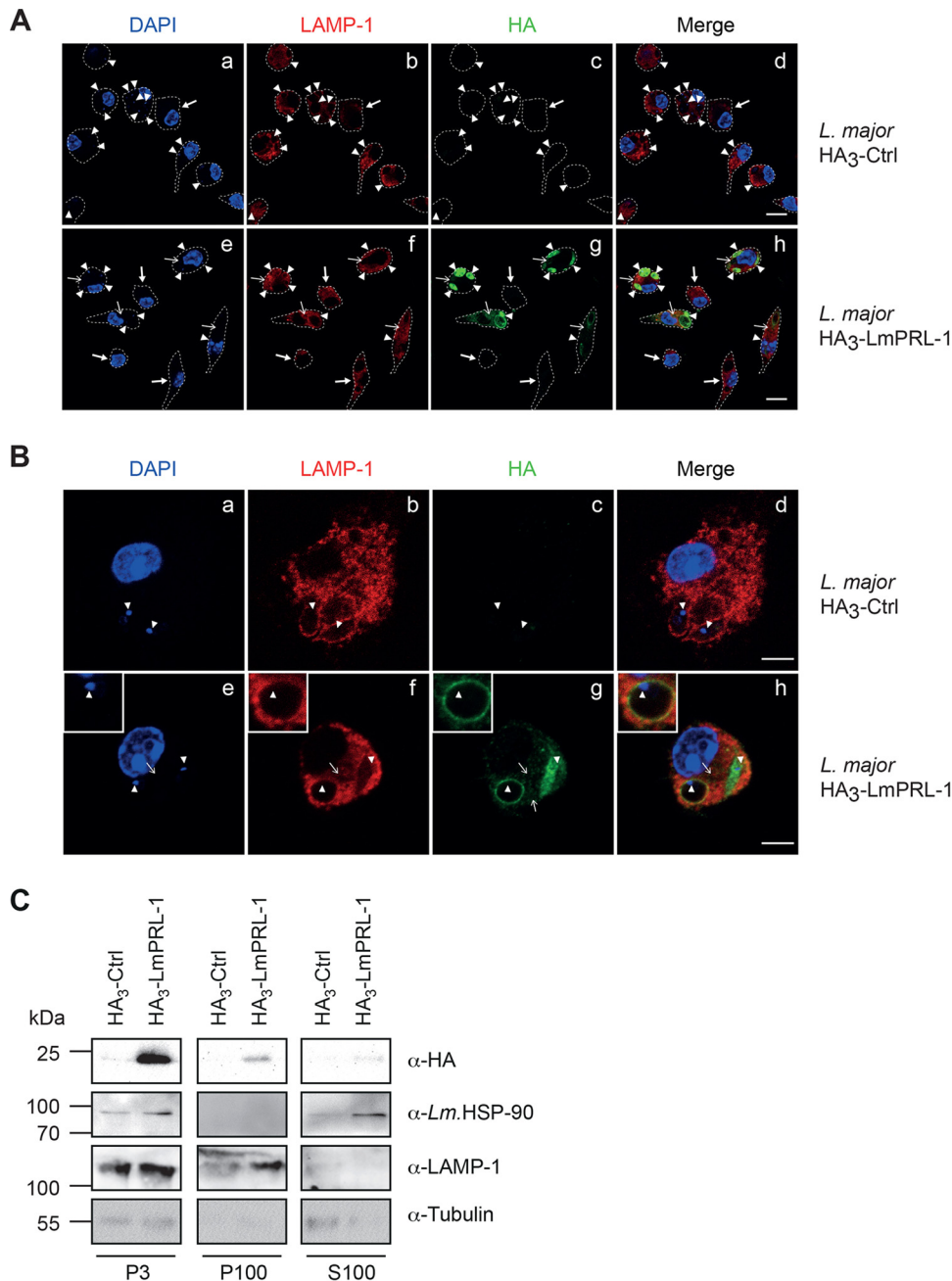


FIG 6 Subcellular localization of HA₃-LmPRL-1 during infection of BMM by *L. major*. (A and B) BMM were infected for 72 h by *L. major* promastigotes carrying the empty plasmid pCLN-3xHA (HA₃-Ctrl) or the plasmid pCLN-3xHA-LmPRL-1 (HA₃-LmPRL-1). Localization of HA-LmPRL-1 (green), the phagosomal marker LAMP-1 (red), and the DNA of the BMM and the parasite (blue) was detected by CLSM. (A) Overview. (B) Single-cell analyses. The dashed white lines delineate the BMM cell shapes. The arrowheads highlight the DNA of the *L. major* kinetoplast. The thin arrows mark the HA-derived signal inside the cytoplasm of the BMM. The thick arrows mark noninfected BMM. Bars, 5 μm. (C) HA₃-LmPRL-1 localization in the cytosolic fraction of BMM during infection. BMM were infected for 72 h with the same parasites as for panel A. The fractions P3 (nucleus and PV), P100 (cytoplasmic membrane and debris), and S100 (cytosol) were analyzed by immunoblotting for the presence of HA-tagged protein, *Leishmania* HSP-90, LAMP-1, and tubulin (from parasites and BMM). The data presented are from one of three experiments with similar results.

BMM infected with *L. major* expressing HA₃-LmPRL-1 contained 2.1 (±0.4)-fold more parasites per 100 cells than the ones infected with control parasites (Fig. 7A). This phenotype largely resulted from an increased parasite number per infected cell (Fig. 7B) and only to a minor degree from a higher percentage of macrophages infected

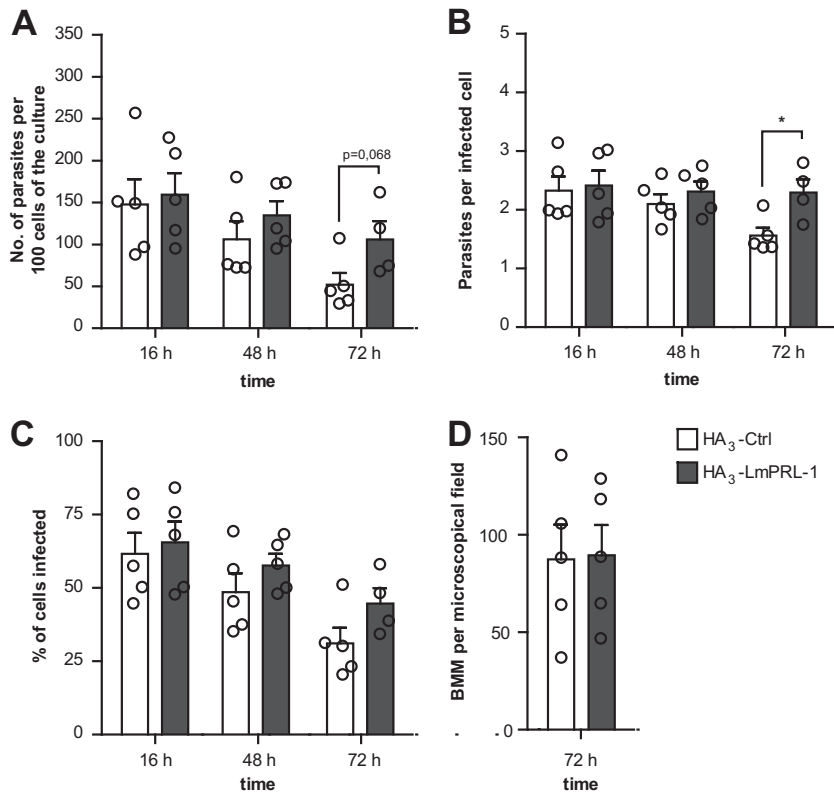


FIG 7 Expression of HA₃-LmPRL-1 increases the infectivity and survival of *L. major* during macrophage infection. (A) Numbers of parasites per 100 cells of a culture. BMM were infected with *L. major* promastigotes (control parasites or parasites expressing HA₃-LmPRL-1) at an MOI of 5. Extracellular parasites were washed away with PBS (2×) after 16 h. At the indicated time points, Diff-Quik staining was performed, and the number of amastigotes per 100 cells was determined (a total of 300 cells/sample). (B) Numbers of parasites per infected macrophage. The number of amastigotes per infected cell was determined as described for panel A. (C) Quantification of the percentage of cells infected. The number of BMM containing one or more parasites was calculated as described for panel A. (D) Quantification of macrophage viability. The number of BMM per microscopic field was calculated as described for panel A. Control parasites are depicted in white, and HA₃-LmPRL-1 in dark gray. The data represent means and standard errors of the mean (SEM) of five experiments. Each circle represents the result of one independent experiment. *, $P < 0.05$.

following expression of HA₃-LmPRL-1 (Fig. 7C). In parallel, the total number of BMM per culture was determined after 72 h of infection in order to see whether the *Leishmania* strains differentially affected host cell survival. The viability of the BMM remained high throughout the course of infection and was independent of the strain of parasite used for infection (Fig. 7D). Altogether, our data suggest that the expression of HA₃-LmPRL-1 phosphatase supports the intracellular survival of *Leishmania* parasites in macrophages.

DISCUSSION

Identifying the virulence factors of *L. major* is crucial for understanding the pathways targeted by the parasite in the mammalian host cell to establish its intracellular habitat. Various surface molecules and secreted proteins of *L. major* parasites have previously been analyzed (15). In the present study, we report the biochemical and functional characterization of a novel *L. major* phosphatase, termed LmPRL-1. We established the expression profile of the endogenous phosphatase during the life cycle of the parasite. Interestingly, we observed that LmPRL-1 was secreted by the parasite. In order to characterize its function, we took advantage of an ectopic expression system, since RNA interference cannot be applied in *L. major* (57, 58). Despite its limitations, this approach revealed the positive effect of LmPRL expression on the survival of *L. major* amastigotes during macrophage infection.

Our analysis of the genome of *L. major* (data not shown) for genes related to LmPRL-1 revealed the presence of a paralogous gene that we named LmPRL-2. A phylogenetic analysis demonstrated that this pair of phosphatases has orthologues in other human-pathogenic *Leishmania* species. This is likely due to a gene duplication event that occurred in a common ancestor of the *Leishmania* species during evolution. The close proximity (6,946 bp apart) of the respective genes for LmPRL-1 and LmPRL-2, [LmjF.16.0230](#) and [LmjF.16.0250](#), on chromosome 16 further supports this notion. The analysis of their sequences also revealed a strong similarity to the mammalian PRL phosphatase family, as illustrated by the conservation of the classical catalytic site (C-X₅-R), a regulatory cysteine at the N terminus, and a farnesylation site at the C terminus. The suspected homology was confirmed by the *in vitro* biochemical characterization of His₆-LmPRL-1 and comparison with the known characteristics of the human PRL-1 (50, 53). First, the catalytic constants (K_m) of His₆-LmPRL-1 using the DiFMUP substrate (9.32×10^{-6} M) was in line with the previously measured value for its human homologue, PRL-1 (4.6×10^{-6} M) (50). In addition, the activity of the phosphatase was shown to be strictly dependent on the reduction of a disulfide bridge formed between its catalytic cysteine and its regulatory cysteine. This reduction allowed a switch between a closed, oxidized, and inactive form and an open, reduced, and active form of the enzyme. Finally, the sensitivity of His₆-LmPRL-1 to oxidation was further confirmed by the enhanced enzymatic activity seen after mutation of the regulatory cysteine. This sensitivity to the redox milieu could be relevant during the oxidative stress encountered by the parasite during infection.

In addition to this biochemical characterization, we also established the expression profile of LmPRL-1 during the growth and stage conversion of *L. major* parasites. Promastigotes already expressed the LmPRL-1 protein in their logarithmic growth phase and maintained this expression during the stationary growth phase. Moreover, LmPRL-1 was still detectable in macrophage lysates even at 72 h after infection with promastigotes, when the parasites had already transformed into amastigotes. This observation on the protein level corroborates and extends recent mRNA expression profiling experiments (59, 60). The expression of the gene [LmjF.16.230](#), coding for LmPRL-1, was upregulated (1.27-fold) during the transition of procyclic into metacyclic promastigotes (59) and after macrophage infection by promastigotes (1.49-fold) (60). However, LmPRL-1 was hardly detectable in macrophages directly infected with amastigotes purified from mouse skin lesions or in lysates of these amastigotes. Altogether, these expression patterns suggest that endogenous LmPRL-1 might play a role during the development of the infective parasite inside its sand fly vector and/or during the initiation and early stages of infection of mammalian phagocytes. Later, endogenous LmPRL-1 expression might steadily decline following the promastigote-to-amastigote transition, possibly due to the upregulation of other prosurvival mechanisms of the parasite.

In addition to the expression pattern, our study found that LmPRL-1 can be secreted, a key characteristic of many virulence factors. Endogenous LmPRL-1 was detected in exosomes released by WT *L. major* promastigotes. These exosomes are cargo vesicles produced by promastigotes and amastigotes and used as a main secretory pathway (15, 56). They are loaded with cytoplasmic and membrane proteins of the parasite, including known virulence factors, such as the surface protease leishmanolysin (Gp63) or EF-1 α (23, 24, 61). Moreover, exosomes are released within the sand fly gut and are inoculated into the host along with the parasites (62). LmPRL-1 has previously been spotted in a proteomic study that analyzed the content of exosomes produced by *Leishmania donovani* (43) or gp63-null mutants of *L. major* (44). These results led us to investigate the expression and fate of LmPRL-1 during the transition of promastigotes into amastigotes inside macrophages. The subcellular localization of LmPRL-1 was addressed in promastigotes, taking advantage of *L. major* expressing a HA-tagged version of the phosphatase. HA₃-LmPRL-1 appeared to spread across the cytoplasm of the promastigotes (Fig. 1A, arrowhead) in a manner similar to that observed for an LmPRL-1 homologue of *T. brucei* ([Tb927.8.5780](#)) that was fused to enhanced yellow

fluorescent protein (eYFP) (63). In addition to this diffuse localization, HA₃-LmPRL-1 tended to accumulate around the kinetoplasts of promastigotes, a phenotype that was also observed for a homologous enzyme in *T. cruzi*, TcPRL-1, which, however, was not tested for its potential secretion (47). The observed subcellular localization of LmPRL-1 is in line with its secretion by exosomes, as the flagellar pocket is known as the most active region of that secretory pathway (54, 55). In addition, using a mutant of its C-terminal farnesylation motif, we could demonstrate that the association of LmPRL-1 with the kinetoplast was fully dependent on this sequence. Promastigotes expressing an LmPRL-1 mutant that lacked the terminal farnesylation site (HA₃-LmPRL-1-C172S) showed diffuse cytoplasmic staining, as was also observed for a similar mutant of human PRL-1 (64). Interestingly, this mutation did not fully abolish the secretion of the phosphatase by exosomes, suggesting that the exosome loading of LmPRL-1 is independent of its functional farnesylation. One plausible explanation for this observation is the possibility that LmPRL-1 forms trimers, like its human homologue PRL-1. This would allow the HA₃-LmPRL-1-C172S mutant to enter exosomes via its trimerization with endogenous WT LmPRL-1. In order to reach a definitive conclusion, the expression of the HA₃-LmPRL-1-C172S mutant protein should be tested in an *L. major* strain with a genetic deletion of LmPRL-1.

When investigating the spatial distribution of the LmPRL-1 phosphatase during infection of macrophages, we found that ectopically expressed HA₃-LmPRL-1 was detectable in amastigotes but, strikingly, also appeared outside the PV. Similarly to other exosome markers, such as the heat shock proteins HSP70 and HSP90 (43, 61) and the *L. major* virulence factor P46 (65, 66), HA₃-LmPRL-1 was identified inside the cytoplasm of infected macrophages and colocalized with the late phagosomal marker LAMP-1 on the surfaces of PV, where it is ideally positioned to manipulate host cell signaling pathways in favor of the parasite (67). It is possible that LmPRL-1 directly modulates the phosphorylation status of host signaling molecules and thereby also synergizes with other secreted virulence factors of *L. major*. This mode of action would explain the positive effect of ectopic HA₃-LmPRL-1 expression on *L. major* survival during macrophage infection. The secreted HA₃-LmPRL-1, however, might also interact with its mammalian homologues, the PRL phosphatases, which play important roles in cell division and cell motility (64, 68). As PRLs need to form a homotrimer to be fully active (49, 52), the possibility that LmPRL-1 interferes with the process of mammalian PRL trimerization has to be considered. It is tempting to speculate that this leads to altered phagocyte functions.

In conclusion, we have shown that *L. major* expresses a PRL-like phosphatase that, based on ectopic expression analyses, is likely to promote parasite survival during infection of macrophages. In addition, LmPRL-1 is actively secreted by the parasite, ends up outside the PV during macrophage infection, and is therefore prone to modulate host cell functions to the advantage of the parasite. Future studies need to address the functional role of LmPRL-1 *in vivo* using double allelic LmPRL-1 knockout *L. major* parasites.

MATERIALS AND METHODS

Phylogenetic analysis. All the gene sequences were extracted from the TritypDB (69) after a BLAST search for *LmjF.16.0230* homologues. The evolutionary history was inferred using the minimum-evolution (ME) method (70). The optimal tree with a sum of branch lengths of 4.67698312 is shown. The tree is drawn to scale, with branch lengths in the same units as those of the evolutionary distances used to infer the phylogenetic tree. The evolutionary distances were computed using the maximum composite likelihood method (71) and are expressed as the number of base substitutions per site. The ME tree was searched using the close-neighbor interchange (CNI) algorithm (72) at a search level of 1. The neighbor-joining algorithm (73) was used to generate the initial tree. The analysis involved 70 nucleotide sequences. All positions containing gaps and missing data were eliminated. There were a total of 305 positions in the final data set. Evolutionary analyses were conducted in MEGA7.0.18 (74).

Bacteria and growth conditions. *Escherichia coli* strains XL1-Blue(MRF') and BL21(DE3) were used for plasmid construction and for overproduction of His₆-tagged proteins, respectively. The *E. coli* strains were grown in LB medium at 37°C with shaking. When required, the LB medium was complemented with 15 g/liter agar-agar, 100 µg/ml ampicillin (Amp), 25 µg/ml kanamycin (Kan), and 15 µg/ml tetracycline (Tet).

Parasites and growth conditions. *L. major* promastigotes (strain MHOM/IL/81/FEBNI) (45) were cultivated at 28°C and 5% CO₂-95% humidified air in modified complete Schneider's medium, which was prepared by supplementation of Schneider's *Drosophila* insect cell medium (Genaxxon Bioscience; pH adjusted to 6.9 after addition of 4.76 mM NaHCO₃, 5.4 mM CaCl₂ · 2H₂O, 50 mM NaOH, and 35 mM HCl) with 100 U/ml penicillin G, 100 µg/ml streptomycin, 1 mM sodium pyruvate, 2 mM L-glutamine, 0.27 mM L-asparagine, 0.55 mM L-arginine, 10 mM HEPES, 2% (vol/vol) normal human urine, and 10% (vol/vol) heat-inactivated fetal calf serum (FCS) in a modification of a protocol previously published by Lima et al. (75). When required, Geneticin (G418) was added to the culture medium at a concentration of 30 µg/ml. *L. major* amastigotes were isolated from skin lesions of the footpads of BALB/c mice at day 30 of subcutaneous infection (76). Animal care and experiments were conducted in accordance with German regulations after local governmental approval (Ansbach, Germany).

Cloning of expression vectors. The genes *LmjF.16.0230* and *LmjF.16.0250* were amplified by PCR with Phusion Hot Start II DNA Polymerase (Thermo Fisher Scientific) using genomic DNA of *L. major* (strain MHOM/IL/81/FEBNI) and specific primers to which appropriate restriction sites had been added (see Table S2 in the supplemental material). The PCR product of *LmjF.16.0230* was inserted into the pET15b vector for affinity purification of the His₆-tagged proteins. For ectopic expression in *L. major*, the *LmjF.16.0230* and *LmjF.16.0250* genes were inserted into the pCLN-3xHA vector, where the expression of the gene of interest was under the control of intergenic regions of *cbp2* genes of *Leishmania mexicana* on the 5' end and *lpg1* of *Leishmania infantum* on the 3' end (77). A list of the plasmids used in this study is presented in Table S1. The nucleotide sequences of all the synthesized and mutated genes were checked to ensure error-free amplification with the T7 or pCLN-3xHA primer pairs for the related plasmids (see Table S2).

Site-directed mutagenesis. Site-directed mutagenesis was carried out following a PCR-based amplification protocol as previously described (78). Briefly, pairs of complementary primers carrying the desired mutation were used to amplify whole pET15b- or pCLN-3xHA-LmPRL plasmids (see Table S2 in the supplemental material). Plasmids used as the matrix carrying the wild-type gene were then digested with DpnI for 15 min at 37°C, followed by incubation for 5 min at 80°C to inactivate the DpnI. Mutated plasmids (see Table S1) were transformed into competent *E. coli* XL1-Blue(MRF') bacteria. For each mutation reaction, plasmids from clones were prepared and sequenced. The success rate of this method approached 66%.

Overexpression and purification of proteins. For each overexpression, competent *E. coli* BL21(DE3) bacteria were freshly transformed with plasmids encoding His₆-PRL-1 (79), His₆-LmPRL-1 WT, or its related mutants. The bacteria were grown overnight in LB supplemented with Amp and Tet and reinoculated at 1:100 in 500 ml LB with Amp and Tet the following day. At an optical density at 600 nm (OD₆₀₀) of 0.5, protein overexpression was induced for 3 h by addition of 1 mM IPTG (isopropyl-β-D-thiogalactopyranoside). The bacteria were centrifuged for 15 min at 8,000 rpm and washed once with purification buffer. Purification with Ni-NTA beads (Qiagen) was performed according to the manufacturer's protocol. Purified fractions were collected and dialyzed overnight against a buffer containing 20 mM Tris-HCl, pH 7.5, 500 mM NaCl, 20% glycerol, 5 mM β-mercaptoethanol and placed at 4°C or -20°C for longer storage (80).

Protein migration assay. Purified His₆-LmPRL was incubated for 1 h with 10 mM either reducing or oxidized DTT (53) and then separated on nonreducing SDS-PAGE. Proteins were detected by Coomassie brilliant blue staining.

Phosphatase assays. Phosphatase activity against *p*NPP was measured by incubating 0.2 mg/ml of His₆-LmPRL-1 with 10 mM *p*NPP for 1 h at 37°C in a buffer (pH 6.0) consisting of 100 mM sodium citrate and 1 mM EDTA. The analyzed proteins were previously incubated or not for 1 h at 4°C with 10 mM reducing DTT. The appearance of yellow *para*-nitrophenol (*p*NP) was measured on a spectrophotometer (λ = 405 nm) after the reaction was arrested by the addition of 1/3 reaction volume of 4 M NaOH (81). Phosphatase activity against DiFMUP was measured by incubating either 67 µg/ml (activity of the mutant) or 25 µg/ml (optimal pH and kinetic constant determination) of His₆-LmPRL-1 with 200 µM DiFMUP (LifeTechnologies) for 20 min at 37°C (50). The appearance of fluorogenic DiFMU was measured on a spectrofluorometer (Fluoroskan Ascent FL; Thermo Fisher Scientific) with the appropriate filter set (excitation [ex]/emission [em], 355 nm/460 nm). For determination of the optimal pH of the enzyme, buffer containing 100 mM sodium citrate and 1 mM EDTA was used at a pH range from 4.0 to 6.5, whereas buffer containing 50 mM HEPES and 1 mM EDTA was used for pH values between 7.0 and 9.0.

Ectopic expression of HA₃-LmPRL in *L. major*. In order to ectopically express HA₃-LmPRL, *L. major* promastigotes were electroporated with pCLN-3xHA-LmPRL vectors following a previously described protocol (77). Briefly, endotoxin-free plasmid DNA was prepared using a NucleoBond Xtra Midi EF plasmid DNA purification kit (Macherey-Nagel). Fifty micrograms of DNA was precipitated with ethanol and rehydrated with 40 µl of sterile electroporation buffer, pH 7.05 (21 mM HEPES, 0.7 mM Na₂HPO₄, 5 mM KCl, 137 mM NaCl, and 6 mM glucose). Promastigote parasites reaching late log phase in modified complete Schneider's medium were washed with cold phosphate-buffered saline (PBS) and electroporation buffer before being resuspended in electroporation buffer at a density of 1.0 × 10⁸ cells/ml. For each electroporation, 0.4 ml of parasite suspension and the dissolved DNA were mixed in a 4-mm-wide, prechilled, sterile electroporation cuvette. Mock electroporation of the parasites without plasmid was carried out in parallel. Electroporation of the cells was done using a Bio-Rad Gene Pulser with 3 pulses at 3,750 V/cm, 25 µF, and 200 Ω. After electroporation, the cells were kept on ice for 10 min and then transferred into 10 ml of complete Schneider's medium. After 24 h, G418 was added, and selection of transfected parasites proceeded until the mock-transfected cells died.

Culture and *in vitro* infection of BMM. BMM were generated as previously described (82). Briefly, the femur and tibia of a female C57BL/6N mouse were removed and flushed with Dulbecco's modified Eagle's medium (DMEM), and 6.0×10^6 nucleated bone marrow cells were grown in 50 ml conditioned DMEM (supplemented with penicillin-streptomycin, 10% [vol/vol] FCS, 50 μ M 2-mercaptoethanol, 1% [vol/vol] 100 \times nonessential amino acids, and 15% [vol/vol] SN from L929 fibroblast cultures [ATCC clone CCL-1] as a source of macrophage colony-stimulating factor) in Teflon bags for 8 days at 37°C and 10% CO₂-90% humidified air. For infection, BMM were seeded in RPMI 1640 (ThermoFisher Scientific no. 21875, supplemented with 10 mM HEPES, 50 μ M 2-mercaptoethanol, 100 U/ml penicillin, 100 μ g/ml streptomycin, and 10% [vol/vol] heat-inactivated FCS) either on glass coverslips in 24-well plates (4.0×10^5 cells/well) or in 6-well plates (3.0×10^6 cells/well). After adherence, the cells were infected with stationary-phase *L. major* WT or HA₃-Ctrl or HA₃-LmPRL promastigotes at an MOI of 5. After 16 h, extracellular parasites were removed by three washes with warm PBS. Samples for Diff-Quick staining were taken at 16 h, 48 h, and 72 h after infection. The infection rate (percentage of cells infected) and the number of parasites per infected cell were determined microscopically (100 \times oil objective; 300 cells in total per condition).

Production of rabbit anti-LmPRL-1 peptide antiserum and immunoblot analysis. To allow specific detection of LmPRL-1, rabbits were immunized with the peptide CQ₁₅₆MHWITKYKRRHQG₁₆₉-amide (Biogenes, Berlin, Germany) coupled to *Limulus polyphemus* hemocyanin (LPH). The serum of the rabbit was then used for immunoblot detection at a dilution of 1:500. Protein samples were prepared from either 5.0×10^7 *L. major* parasites or 3.0×10^6 BMM, which were lysed in 200 μ l or 60 μ l of ice-cold Frackelton buffer (10 mM Tris, 50 mM NaCl, 30 mM sodium pyrophosphate, 1% Triton X-100, 1 mM DTT, 1 mM phenylmethylsulfonyl fluoride [PMSF], protease inhibitor cocktail broad range [Roth], and 10 mM phenanthroline for the parasite samples), respectively. In addition, *Leishmania* lysates were sonicated for 5 min (power, H; interval, 0.5) in a Bioruptor water bath (Diagenode). All the samples were then centrifuged at $14,000 \times g$ for 10 min at 4°C. Protein quantities of the supernatants were determined by the Bradford method (Roti-Quant; Roth). Lysates were separated by SDS-15% PAGE and transferred to a nitrocellulose membrane (pore size, 0.2 μ m) using a semidry blotter (Bio-Rad). To block nonspecific binding sites, the blotted membranes were placed in Tris-buffered saline (TBS) with 5% nonfat dry milk and 0.05% Tween 20 for at least 1 h. For detection of the target proteins, the blots were analyzed by enhanced chemiluminescence (RotiLumin; Roth) using different primary Abs and the respective horseradish peroxidase (HRP)-conjugated secondary Ab. Mouse anti-HA Ab (diluted 1:1,000; clone 16B12; Covance), rabbit anti- α -actin Ab (diluted 1:1,000; A2066; Sigma-Aldrich), mouse anti- α -tubulin Ab (diluted 1:1,000; clone B-5-2-1; Sigma-Aldrich), rat anti-LAMP-1 (diluted 1:1,000; clone 1D4B; DSHB), and chicken anti-*Leishmania* HSP90 and HSP70 sera (diluted 1:500) (83) were used as primary Abs. Anti-mouse IgG Ab (diluted 1:5,000; Roth), anti-rat IgG Ab (diluted 1:10,000; Jackson ImmunoResearch), anti-rabbit IgG Ab (diluted 1:2,500; Roth), and anti-chicken IgG Ab (diluted 1:10,000; Dianova) were used as HRP-conjugated secondary Abs. The intensities of the obtained protein bands were determined with Image J software (84).

CLSMF. For *L. major* samples, promastigotes were grown to stationary phase before washing with PBS and subsequent fixation in 4% paraformaldehyde (PFA) (Alfa Aesar) for 20 min at room temperature (RT) in the dark. Fixed promastigotes were seeded on poly-L-lysine (Sigma-Aldrich)-coated glass coverslips (24-well plate; 2.5×10^5 to 5×10^5 cells/well), dried for 15 min, washed with PBS, and permeabilized with ice-cold methanol for 1 min. For BMM samples, the cells that were seeded on glass coverslips (24-well plate; 0.4×10^6 cells/well) were washed, fixed, and permeabilized in a similar way. All the samples were then washed for 15 min with 0.1% Tween 20 in PBS (PBST) and blocked for 30 min with 5% donkey serum (Dianova), 0.1% saponin in PBS. After three washing steps of 5 min each with PBST, the cells were incubated with a primary Ab diluted in 0.5% donkey serum in PBS for 1 to 2 h at RT, followed by another three washing steps and incubation with a related secondary Ab diluted in 0.5% donkey serum in PBS for 1 h at RT in the dark. After three final washings, the cells were mounted with Molecular Probes ProLong Gold Antifade Mountant (Life Technologies), containing DAPI (4',6-diamidino-2-phenylindole) to stain DNA, on coverslips and cured overnight. Mouse anti-HA Ab (diluted 1:500; clone 16B12; Covance), rat anti-LAMP-1 (diluted 1:600; clone 1D4B; DSHB), and polyclonal human anti-*Leishmania* serum (diluted 1:1,000; derived from a patient with multilesional cutaneous leishmaniasis due to *L. infantum* infection [85]) were used as primary Abs. Goat anti-mouse IgG Ab coupled to Alexa 488 (diluted 1:400; Dianova), goat anti-mouse IgG Ab coupled to Alexa 594 (diluted 1:1,600; Dianova), donkey anti-rat IgG Ab coupled to Cy5 (diluted 1:400; Dianova), goat-anti-human IgG coupled to Alexa 488 (diluted 1:1,600; Jackson ImmunoResearch), and goat-anti-human IgG coupled to Alexa 647 (diluted 1:100; Jackson ImmunoResearch) were used as secondary Abs. The slides were analyzed with a confocal microscope (LSM 700; Zeiss) using a 405-nm, 488-nm, 555-nm, or 639-nm laser line. Processing of the images was done with ZEN software 2009 (Zeiss).

Purification of exosomes generated by *L. major* promastigotes. Exosome isolation was performed as described previously (61) with minor modification. Briefly, *L. major* promastigotes were grown to stationary phase (5.0×10^7 cells/ml) in 150 ml modified complete Schneider's medium supplemented with 30 μ g/ml G418 for pCLN-3xHA-containing strains. Twenty-four hours before exosome isolation, the parasites were washed with PBS and kept in RPMI 1640 supplemented with penicillin and streptomycin but without G418 and FCS for 24 h (to avoid contamination by serum proteins). The parasite cultures were then centrifuged for 10 min at $1,000 \times g$. The supernatants were centrifuged at $1,000 \times g$ for 30 min, followed by another centrifugation at $15,000 \times g$ for 45 min to remove dead parasites and debris. Finally, the supernatants were ultracentrifuged at $110,000 \times g$ for 1 h to pellet the exosomes. All centrifugation steps were done at 4°C. The exosomes were finally resuspended in 50 to 100 μ l PBS and

subjected to trypsin digestion (50 $\mu\text{g}/\text{ml}$) in the presence of 0.3% Triton X-100 (preincubation for 5 min on ice) at 37°C for 30 min. Samples were then analyzed by immunoblotting.

Electron microscopy. For electron microscopy, exosomes collected from 50 ml of parasite culture grown under conditions similar to those for exosome preparation were directly resuspended in 2.5% glutaraldehyde in cacodylate buffer (0.1 M, pH 7.3) containing 0.1 M glucose and stored at 4°C until further sample preparation. For negative-contrast staining, Formvar-film, carbon-coated, 400-mesh copper grids were prepared and hydrophilized by glow discharge in a high-vacuum coating system (Med 020; Bal-Tec AG, Liechtenstein) immediately before use. Grids were floated with the coated side on a 30- μl drop of the exosome suspension for 10 min, placed on a drop of 10% aqueous uranyl acetate for contrast for 10 min, and briefly dried on filter paper. They were viewed in a FEI Tecnai 12 transmission electron microscopy (TEM) at 80 kV and imaged using electron image film (SO-163; Carestream, USA). The developed film plates were digitized on a scanner (Epson Perfection V700 photo scanner) and processed using Adobe Photoshop CS3.

Subcellular fractionation. BMM were infected at an MOI of 5 with *L. major* promastigotes. Extracellular parasites were washed away with PBS (2 \times) after 16 h. After 72 h, the cells were washed with Hanks' balanced salt solution. The cells were treated with cold hypotonic buffer (20 mM Tris, pH 7.5) containing protease inhibitors and passed 50 times through a 22-gauge needle to disrupt their cytosolic membranes. The nucleus and large organelles were removed by centrifugation at 3,000 $\times g$ (P3), and the supernatants were supplemented with NaCl to a final concentration of 0.15 M. The cytosolic fractions were prepared further by centrifuging the supernatants at 100,000 $\times g$ for 1 h at 4°C. The supernatants were considered cytosolic fractions (S100), whereas the pellets represented the small organelles and the cytoplasmic membrane (P100).

Statistical analysis. Data sets were analyzed using the unpaired, two-tailed Student *t* test. Significance was evaluated by measuring the *P* value.

SUPPLEMENTAL MATERIAL

Supplemental material for this article may be found at <https://doi.org/10.1128/IAI.00084-17>.

SUPPLEMENTAL FILE 1, PDF file, 0.2 MB.

ACKNOWLEDGMENTS

We are grateful to Lisa Wirker for preparation of samples and Wolfram Maginot for photographic support for TEM. We also thank Anja Lührmann (UK Erlangen, Germany) for scientific advice and reagents and Jennifer S. Laurence (University of Kansas, USA) for providing reagents.

This study was supported by the German Research Foundation (DFG) (grant SO 1149/1-1 to D.S.; grant CRC1181, project C05, to C.B.), by the Interdisciplinary Center for Clinical Research (IZKF) of the Medical Faculty of the FAU Erlangen-Nürnberg (project grants A61 and A63 to C.B.), and by the Robert Pflieger Stiftung Bamberg (project grant to C.B.). D.S. acknowledges his position as an associated researcher within the CRC796.

D.S. conceived and coordinated the study. S.L., E.M.L.-T., and D.S. designed and performed experiments and analyzed data. J.C. provided vectors and know-how for generating the transgenic *Leishmania* strains. C.B. and U.S. provided technical expertise on the macrophage infection experiments and contributed significantly to the conception and design of the study. D.S., S.L., and C.B. wrote the manuscript.

We declare that we have no conflict of interest.

REFERENCES

- Akhoundi M, Kuhls K, Cannet A, Votýpka J, Marty P, Delaunay P, Sereno D. 2016. A historical overview of the classification, evolution, and dispersion of *Leishmania* parasites and sandflies. *PLoS Negl Trop Dis* 10: e0004349. <https://doi.org/10.1371/journal.pntd.0004349>.
- Kaye P, Scott P. 2011. Leishmaniasis: complexity at the host-pathogen interface. *Nat Rev Microbiol* 9:604–615. <https://doi.org/10.1038/nrmicro2608>.
- Murray HW, Berman JD, Davies CR, Saravia NG. 2005. Advances in leishmaniasis. *Lancet* 366:1561–1577. [https://doi.org/10.1016/S0140-6736\(05\)67629-5](https://doi.org/10.1016/S0140-6736(05)67629-5).
- Bogdan C. 2012. Leishmaniasis in rheumatology, haematology and oncology: epidemiological, immunological and clinical aspects and caveats. *Ann Rheum Dis* 71(Suppl 2):i60–i66. <https://doi.org/10.1136/annrheumdis-2011-200596>.
- Savoia D. 2015. Recent updates and perspectives on leishmaniasis. *J Infect Dev Ctries* 9:588–596. <https://doi.org/10.3855/jidc.6833>.
- Depledge DP, Evans KJ, Ivens AC, Aziz N, Maroof A, Kaye PM, Smith DF. 2009. Comparative expression profiling of *Leishmania*: modulation in gene expression between species and in different host genetic backgrounds. *PLoS Negl Trop Dis* 3:e476. <https://doi.org/10.1371/journal.pntd.0000476>.
- Silva-Almeida M, Souza-Silva F, Pereira BAS, Ribeiro-Guimarães ML, Alves CR. 2014. Overview of the organization of protease genes in the genome of *Leishmania* spp. *Parasit Vectors* 7:387. <https://doi.org/10.1186/1756-3305-7-387>.
- McCall L-I, Matlashewski G. 2010. Localization and induction of the A2 virulence factor in *Leishmania*: evidence that A2 is a stress response

- protein. *Mol Microbiol* 77:518–530. <https://doi.org/10.1111/j.1365-2958.2010.07229.x>.
9. Zhu Y, Davis A, Smith BJ, Curtis J, Handman E. 2009. Leishmania major CorA-like magnesium transporters play a critical role in parasite development and virulence. *Int J Parasitol* 39:713–723. <https://doi.org/10.1016/j.ijpara.2008.11.010>.
 10. Morales MA, Pescher P, Späth GF. 2010. Leishmania major MPK7 protein kinase activity inhibits intracellular growth of the pathogenic amastigote stage. *Eukaryot Cell* 9:22–30. <https://doi.org/10.1128/EC.00196-09>.
 11. Norris-Mullins B, VanderKolk K, Vacchina P, Joyce MV, Morales MA. 2014. LmaPA2G4, a homolog of human Ebp1, is an essential gene and inhibits cell proliferation in *L. major*. *PLoS Negl Trop Dis* 8:e2646. <https://doi.org/10.1371/journal.pntd.0002646>.
 12. Bogdan C, Rölinghoff M. 1998. The immune response to Leishmania: mechanisms of parasite control and evasion. *Int J Parasitol* 28:121–134. [https://doi.org/10.1016/S0020-7519\(97\)00169-0](https://doi.org/10.1016/S0020-7519(97)00169-0).
 13. Bogdan C. 2008. Mechanisms and consequences of persistence of intracellular pathogens: leishmaniasis as an example. *Cell Microbiol* 10:1221–1234. <https://doi.org/10.1111/j.1462-5822.2008.01146.x>.
 14. Shio MT, Hassani K, Isnard A, Ralph B, Contreras I, Gomez MA, Abu-Dayyeh I, Olivier M. 2012. Host cell signalling and Leishmania mechanisms of evasion. *J Trop Med* 2012:1–14. <https://doi.org/10.1155/2012/819512>.
 15. Lambertz U, Silverman JM, Nandan D, McMaster WR, Clos J, Foster LJ, Reiner NE. 2012. Secreted virulence factors and immune evasion in visceral leishmaniasis. *J Leukoc Biol* 91:887–899. <https://doi.org/10.1189/jlb.0611326>.
 16. Atayde VD, Hassani K, da Silva Lira Filho A, Borges AR, Adhikari A, Martel C, Olivier M. 2016. Leishmania exosomes and other virulence factors: impact on innate immune response and macrophage functions. *Cell Immunol* 309:7–18. <https://doi.org/10.1016/j.cellimm.2016.07.013>.
 17. Richardson JM, Morrison LS, Bland ND, Bruce S, Coombs GH, Mottram JC, Walkinshaw MD. 2009. Structures of Leishmania major orthologues of macrophage migration inhibitory factor. *Biochem Biophys Res Commun* 380:442–448. <https://doi.org/10.1016/j.bbrc.2009.01.030>.
 18. Holowka T, Castilho TM, Garcia AB, Sun T, McMahon-Pratt D, Bucala R. 2016. Leishmania-encoded orthologs of macrophage migration inhibitory factor regulate host immunity to promote parasite persistence. *FASEB J* 30:2249–2265. <https://doi.org/10.1096/fj.201500189R>.
 19. Späth GF, Epstein L, Leader B, Singer SM, Avila HA, Turco SJ, Beverley SM. 2000. Lipophosphoglycan is a virulence factor distinct from related glycoconjugates in the protozoan parasite Leishmania major. *Proc Natl Acad Sci U S A* 97:9258–9263. <https://doi.org/10.1073/pnas.160257897>.
 20. Madeira da Silva L, Owens KL, Murta SMF, Beverley SM. 2009. Regulated expression of the Leishmania major surface virulence factor lipophosphoglycan using conditionally destabilized fusion proteins. *Proc Natl Acad Sci U S A* 106:7583–7588. <https://doi.org/10.1073/pnas.0901698106>.
 21. Desjardins M, Descoteaux A. 1997. Inhibition of phagolysosomal biogenesis by the Leishmania lipophosphoglycan. *J Exp Med* 185:2061–2068. <https://doi.org/10.1084/jem.185.12.2061>.
 22. Vinet AF, Fukuda M, Turco SJ, Descoteaux A. 2009. The Leishmania donovani lipophosphoglycan excludes the vesicular proton-ATPase from phagosomes by impairing the recruitment of synaptotagmin V. *PLoS Pathog* 5:e1000628. <https://doi.org/10.1371/journal.ppat.1000628>.
 23. Olivier M, Atayde VD, Isnard A, Hassani K, Shio MT. 2012. Leishmania virulence factors: focus on the metalloprotease GP63. *Microbes Infect* 14:1377–1389. <https://doi.org/10.1016/j.micinf.2012.05.014>.
 24. Nandan D, Yi T, Lopez M, Lai C, Reiner NE. 2002. Leishmania EF-1alpha activates the Src homology 2 domain containing tyrosine phosphatase SHP-1 leading to macrophage deactivation. *J Biol Chem* 277:50190–50197. <https://doi.org/10.1074/jbc.M209210200>.
 25. Blanchette J, Racette N, Faure R, Siminovitsh KA, Olivier M. 1999. Leishmania-induced increases in activation of macrophage SHP-1 tyrosine phosphatase are associated with impaired IFN-gamma-triggered JAK2 activation. *Eur J Immunol* 29:3737–3744. [https://doi.org/10.1002/\(SICI\)1521-4141\(199911\)29:11<3737::AID-IMMU3737>3.0.CO;2-5](https://doi.org/10.1002/(SICI)1521-4141(199911)29:11<3737::AID-IMMU3737>3.0.CO;2-5).
 26. Gomez MA, Contreras I, Hallé M, Tremblay ML, McMaster RW, Olivier M. 2009. Leishmania GP63 alters host signaling through cleavage-activated protein tyrosine phosphatases. *Sci Signal* 2:ra58–ra58. <https://doi.org/10.1126/scisignal.2000213>.
 27. Bhattacharyya S, Ghosh S, Sen P, Roy S, Majumdar S. 2001. Selective impairment of protein kinase C isotypes in murine macrophage by Leishmania donovani. *Mol Cell Biochem* 216:47–57. <https://doi.org/10.1023/A:1011048210691>.
 28. Pingel S, Wang ZE, Locksley RM. 1998. Distribution of protein kinase C isoforms after infection of macrophages with Leishmania major. *Infect Immun* 66:1795–1799.
 29. Nandan D, Lo R, Reiner NE. 1999. Activation of phosphotyrosine phosphatase activity attenuates mitogen-activated protein kinase signaling and inhibits c-FOS and nitric oxide synthase expression in macrophages infected with Leishmania donovani. *Infect Immun* 67:4055–4063.
 30. Soares-Silva M, Diniz FF, Gomes GN, Bahia D. 2016. The mitogen-activated protein kinase (MAPK) pathway: role in immune evasion by trypanosomatids. *Front Microbiol* 7:183. <https://doi.org/10.3389/fmicb.2016.00183>.
 31. Nandan D, Reiner NE. 1995. Attenuation of gamma interferon-induced tyrosine phosphorylation in mononuclear phagocytes infected with Leishmania donovani: selective inhibition of signaling through Janus kinases and Stat1. *Infect Immun* 63:4495–4500.
 32. Shio MT, Olivier M. 2010. Leishmania survival mechanisms: the role of host phosphatases. *J Leukoc Biol* 88:1–3. <https://doi.org/10.1189/jlb.0210088>.
 33. Szöör B. 2010. Trypanosomatid protein phosphatases. *Mol Biochem Parasitol* 173:53–63. <https://doi.org/10.1016/j.molbiopara.2010.05.017>.
 34. Gottlieb M, Dwyer DM. 1981. Protozoan parasite of humans: surface membrane with externally disposed acid phosphatase. *Science* 212:939–941. <https://doi.org/10.1126/science.7233189>.
 35. Remaley AT, Das S, Campbell PI, LaRocca GM, Pope MT, Glew RH. 1985. Characterization of Leishmania donovani acid phosphatases. *J Biol Chem* 260:880–886.
 36. Shakarian AM, Joshi MB, Yamage M, Ellis SL, Debrabant A, Dwyer DM. 2003. Members of a unique histidine acid phosphatase family are conserved amongst a group of primitive eukaryotic human pathogens. *Mol Cell Biochem* 245:31–41. <https://doi.org/10.1023/A:1022851914014>.
 37. Remaley AT, Kuhns DB, Basford RE, Glew RH, Kaplan SS. 1984. Leishmanial phosphatase blocks neutrophil O-2 production. *J Biol Chem* 259:11173–11175.
 38. Papadaki A, Politou AS, Smirlis D, Kotini MP, Kourou K, Papamarcaki T, Boleti H. 2015. The Leishmania donovani histidine acid ectophosphatase LdMACP: insight into its structure and function. *Biochem J* 467:473–486. <https://doi.org/10.1042/BJ20141371>.
 39. Fernandes ACS, Soares DC, Saraiva EM, Meyer-Fernandes JR, Souto-Padrón T. 2013. Different secreted phosphatase activities in Leishmania amazonensis. *FEMS Microbiol Lett* 340:117–128. <https://doi.org/10.1111/1574-6968.12080>.
 40. Aoun K, Bouratbine A. 2014. Cutaneous leishmaniasis in North Africa: a review. *Parasite* 21:14. <https://doi.org/10.1051/parasite/2014014>.
 41. Alvar J, Vélez ID, Bern C, Herrero M, Desjeux P, Cano J, Jannin J, den Boer M, WHO Leishmaniasis Control Team. 2012. Leishmaniasis worldwide and global estimates of its incidence. *PLoS One* 7:e35671. <https://doi.org/10.1371/journal.pone.0035671>.
 42. Rios P, Li X, Köhn M. 2013. Molecular mechanisms of the PRL phosphatases. *FEBS J* 280:505–524. <https://doi.org/10.1111/j.1742-4658.2012.08565.x>.
 43. Silverman JM, Clos J, deOliveira CC, Shirvani O, Fang Y, Wang C, Foster LJ, Reiner NE. 2010. An exosome-based secretion pathway is responsible for protein export from Leishmania and communication with macrophages. *J Cell Sci* 123:842–852. <https://doi.org/10.1242/jcs.056465>.
 44. Hassani K, Shio MT, Martel C, Faubert D, Olivier M. 2014. Absence of metalloprotease GP63 alters the protein content of Leishmania exosomes. *PLoS One* 9:e95007. <https://doi.org/10.1371/journal.pone.0095007>.
 45. Solbach W, Forberg K, Rölinghoff M. 1986. Effect of T-lymphocyte suppression on the parasite burden in Leishmania major-infected, genetically susceptible BALB/c mice. *Infect Immun* 54:909–912.
 46. Ivens AC, Peacock CS, Worthey EA, Murphy L, Aggarwal G, Berriman M, Sisk E, Rajandream M-A, Adlem E, Aert R, Anupama A, Apostoluz T, Atzippe P, Bason N, Bauser C, Beck A, Beverley SM, Bianchettin G, Borzym K, Bothe G, Bruschi CV, Collins M, Cadag E, Ciarloni L, Clayton C, Coulson RMR, Cronin A, Cruz AK, Davies RM, De Gaudenzi J, Dobson DE, Duesterhoeft A, Fazelina G, Fosker N, Frasch AC, Fraser A, Fuchs M, Gabel C, Goble A, Goffeau A, Harris D, Hertz-Fowler C, Hilbert H, Horn D, Huang Y, Klages S, Knights A, Kube M, Larke N, Litvin L, Lord A, Louie T, Marra M, Masuy D, Matthews K, Michaeli S, Mottram JC, Müller-Auer S, Munden H, Nelson S, Norbertczak H, Oliver K, O'Neil S, Pentony M, Pohl TM, Price C, Purnelle B, Quail MA, Rabbinowitsch E, Reinhardt R, Rieger M, Rinta J, Robben J, Robertson L, Ruiz JC, Rutter S, Saunders D, Schäfer M, Schein J, Schwartz DC, Seeger K, Seyler A, Sharp S, Shin H, Sivam D, Squares R, Squares S, Tosato V, Vogt C, Volckaert G, Wambutt R, Warren T, Wedler H, Woodward J, Zhou S, Zimmermann W, Smith DF, Blackwell JM, Stuart KD, Barrell B,

- Myler PJ. 2005. The genome of the kinetoplastid parasite, *Leishmania major*. *Science* 309:436–442. <https://doi.org/10.1126/science.1112680>.
47. Cuevas IC, Rohloff P, Sanchez DO, Docampo R. 2005. Characterization of farnesylated protein tyrosine phosphatase TcPRL-1 from *Trypanosoma cruzi*. *Eukaryot Cell* 4:1550–1561. <https://doi.org/10.1128/EC.4.9.1550-1561.2005>.
 48. Alsford S, Turner DJ, Obado SO, Sanchez-Flores A, Glover L, Berriman M, Hertz-Fowler C, Horn D. 2011. High-throughput phenotyping using parallel sequencing of RNA interference targets in the African trypanosome. *Genome Res* 21:915–924. <https://doi.org/10.1101/gr.115089.110>.
 49. Jeong D, Kim S, Kim J, Son J, Park M, Lim S, Yoon T-S, Ryu S. 2005. Trimeric structure of PRL-1 phosphatase reveals an active enzyme conformation and regulation mechanisms. *J Mol Biol* 345:401–413. <https://doi.org/10.1016/j.jmb.2004.10.061>.
 50. Sun J-P, Wang W-Q, Yang H, Liu S, Liang F, Fedorov AA, Almo SC, Zhang Z-Y. 2005. Structure and biochemical properties of PRL-1, a phosphatase implicated in cell growth, differentiation, and tumor invasion. *Biochemistry* 44:12009–12021. <https://doi.org/10.1021/bi0509191>.
 51. Ishii T, Funato Y, Miki H. 2013. Thioredoxin-related protein 32 (TRP32) specifically reduces oxidized phosphatase of regenerating liver (PRL). *J Biol Chem* 288:7263–7270. <https://doi.org/10.1074/jbc.M112.418004>.
 52. Sun J-P, Luo Y, Yu X, Wang W-Q, Zhou B, Liang F, Zhang Z-Y. 2007. Phosphatase activity, trimerization, and the C-terminal polybasic region are all required for PRL1-mediated cell growth and migration. *J Biol Chem* 282:29043–29051. <https://doi.org/10.1074/jbc.M703537200>.
 53. Skinner A, Vartia A, Williams T, Laurence J. 2009. Enzyme activity of phosphatase of regenerating liver is controlled by the redox environment and its C-terminal residues. *Biochemistry* 48:4262–4272. <https://doi.org/10.1021/bi900241k>.
 54. Silverman JM, Reiner NE. 2011. *Leishmania* exosomes deliver preemptive strikes to create an environment permissive for early infection. *Front Cell Infect Microbiol* 1:26. <https://doi.org/10.3389/fcimb.2011.00026>.
 55. McConville MJ, Mullin KA, Ilgoutz SC, Teasdale RD. 2002. Secretory pathway of trypanosomatid parasites. *Microbiol Mol Biol Rev* 66:122–154. <https://doi.org/10.1128/MMBR.66.1.122-154.2002>.
 56. Silverman JM, Chan SK, Robinson DP, Dwyer DM, Nandan D, Foster LJ, Reiner NE. 2008. Proteomic analysis of the secretome of *Leishmania donovani*. *Genome Biol* 9:R35. <https://doi.org/10.1186/gb-2008-9-2-r35>.
 57. Robinson KA, Beverley SM. 2003. Improvements in transfection efficiency and tests of RNA interference (RNAi) approaches in the protozoan parasite *Leishmania*. *Mol Biochem Parasitol* 128:217–228. [https://doi.org/10.1016/S0166-6851\(03\)00079-3](https://doi.org/10.1016/S0166-6851(03)00079-3).
 58. Kolev NG, Tschudi C, Ullu E. 2011. RNA interference in protozoan parasites: achievements and challenges. *Eukaryot Cell* 10:1156–1163. <https://doi.org/10.1128/EC.05114-11>.
 59. Dillon LAL, Okrah K, Hughitt VK, Suresh R, Li Y, Fernandes MC, Belew AT, Corrada Bravo H, Mosser DM, El-Sayed NM. 2015. Transcriptomic profiling of gene expression and RNA processing during *Leishmania major* differentiation. *Nucleic Acids Res* 43:6799–6813. <https://doi.org/10.1093/nar/gkv656>.
 60. Dillon LAL, Suresh R, Okrah K, Corrada Bravo H, Mosser DM, El-Sayed NM. 2015. Simultaneous transcriptional profiling of *Leishmania major* and its murine macrophage host cell reveals insights into host-pathogen interactions. *BMC Genomics* 16:1108. <https://doi.org/10.1186/s12864-015-2237-2>.
 61. Silverman JM, Clos J, Horakova E, Wang AY, Wiesgigl M, Kelly I, Lynn MA, McMaster WR, Foster LJ, Levings MK, Reiner NE. 2010. *Leishmania* exosomes modulate innate and adaptive immune responses through effects on monocytes and dendritic cells. *J Immunol* 185:5011–5022. <https://doi.org/10.4049/jimmunol.1000541>.
 62. Atayde VD, Aslan H, Townsend S, Hassani K, Kamhawi S, Olivier M. 2015. Exosome secretion by the parasitic protozoan *Leishmania* within the sand fly midgut. *Cell Rep* 13:957–967. <https://doi.org/10.1016/j.celrep.2015.09.058>.
 63. Fritz M, Vanselow J, Sauer N, Lamer S, Goos C, Siegel TN, Subota I, Schlosser A, Carrington M, Kramer S. 2015. Novel insights into RNP granules by employing the trypanosome's microtubule skeleton as a molecular sieve. *Nucleic Acids Res* 43:8013–8032. <https://doi.org/10.1093/nar/gkv731>.
 64. Wang J, Kirby C, Herbst R. 2002. The tyrosine phosphatase PRL-1 localizes to the endoplasmic reticulum and the mitotic spindle and is required for normal mitosis. *J Biol Chem* 277:46659–46668. <https://doi.org/10.1074/jbc.M206407200>.
 65. Reiling L, Chrobak M, Schmetz C, Clos J. 2010. Overexpression of a single *Leishmania major* gene enhances parasite infectivity in vivo and in vitro. *Mol Microbiol* 76:1175–1190. <https://doi.org/10.1111/j.1365-2958.2010.07130.x>.
 66. Bifeld E, Chrobak M, Zander D, Schleicher U, Schönian G, Clos J. 2015. Geographical sequence variation in the *Leishmania major* virulence factor P46. *Infect Genet Evol* 30:195–205. <https://doi.org/10.1016/j.meegid.2014.12.029>.
 67. Liévin-Le Moal V, Loiseau PM. 2016. *Leishmania* hijacking of the macrophage intracellular compartments. *FEBS J* 283:598–607. <https://doi.org/10.1111/febs.13601>.
 68. Zeng Q, Dong JM, Guo K, Li J, Tan H-X, Koh V, Pallen CJ, Manser E, Hong W. 2003. PRL-3 and PRL-1 promote cell migration, invasion, and metastasis. *Cancer Res* 63:2716–2722.
 69. Aslett M, Aurrecochea C, Berriman M, Brestelli J, Brunk BP, Carrington M, Depledge DP, Fischer S, Gajria B, Gao X, Gardner MJ, Gingle A, Grant G, Harb OS, Heiges M, Hertz-Fowler C, Houston R, Innamorato F, Iodice J, Kissinger JC, Kraemer E, Li W, Logan FJ, Miller JA, Mitra S, Myler PJ, Nayak V, Pennington C, Phan I, Pinney DF, Ramasamy G, Rogers MB, Roos DS, Ross C, Sivam D, Smith DF, Srinivasamoorthy G, Stoekert CJ, Subramanian S, Thibodeau R, Tivey A, Treatman C, Velarde G, Wang H. 2010. TriTrypDB: a functional genomic resource for the Trypanosomatidae. *Nucleic Acids Res* 38:D457–D462. <https://doi.org/10.1093/nar/gkp851>.
 70. Rzhetsky A, Nei M. 1992. A simple method for evaluating and testing minimum-evolution trees. *Mol Biol Evol* 9:945–967.
 71. Tamura K, Nei M, Kumar S. 2004. Prospects for inferring very large phylogenies by using the neighbor-joining method. *Proc Natl Acad Sci U S A* 101:11030–11035. <https://doi.org/10.1073/pnas.0404206101>.
 72. Nei M, Kumar S. 2000. *Molecular evolution and phylogenetics*. Oxford University Press, Oxford, United Kingdom.
 73. Saitou N, Nei M. 1987. The neighbor-joining method: a new method for reconstructing phylogenetic trees. *Mol Biol Evol* 4:406–425.
 74. Kumar S, Stecher G, Tamura K. 2016. MEGA7: Molecular Evolutionary Genetics Analysis version 7.0 for bigger datasets. *Mol Biol Evol* 33:1870–1874. <https://doi.org/10.1093/molbev/msw054>.
 75. Lima HC, Bleyenbergh JA, Titus RG. 1997. A simple method for quantifying *Leishmania* in tissues of infected animals. *Parasitol Today* 13:80–82. [https://doi.org/10.1016/S0169-4758\(96\)40010-2](https://doi.org/10.1016/S0169-4758(96)40010-2).
 76. Bogdan C, Streck H, Röllinghoff M, Solbach W. 1989. Cyclosporin A enhances elimination of intracellular *L. major* parasites by murine macrophages. *Clin Exp Immunol* 75:141–146.
 77. Hombach A, Ommen G, Chrobak M, Clos J. 2013. The Hsp90-Sti1 interaction is critical for *Leishmania donovani* proliferation in both life cycle stages. *Cell Microbiol* 15:585–600. <https://doi.org/10.1111/cmi.12057>.
 78. Zheng L, Baumann U, Reymond J-L. 2004. An efficient one-step site-directed and site-saturation mutagenesis protocol. *Nucleic Acids Res* 32:e115. <https://doi.org/10.1093/nar/gnh110>.
 79. Laurence JS, Hallenga K, Stauffacher CV. 2004. ¹H, ¹⁵N, ¹³C resonance assignments of the human protein tyrosine phosphatase PRL-1. *J Biomol NMR* 29:417–418. <https://doi.org/10.1023/B:JNMR.0000032506.16792.c6>.
 80. Soulat D, Jault J-M, Duclos B, Geourjon C, Cozzone AJ, Grangeasse C. 2006. *Staphylococcus aureus* operates protein-tyrosine phosphorylation through a specific mechanism. *J Biol Chem* 281:14048–14056. <https://doi.org/10.1074/jbc.M513600200>.
 81. Soulat D, Vaganay E, Duclos B, Genestier A-L, Etienne J, Cozzone AJ. 2002. *Staphylococcus aureus* contains two low-molecular-mass phosphotyrosine protein phosphatases. *J Bacteriol* 184:5194–5199. <https://doi.org/10.1128/JB.184.18.5194-5199.2002>.
 82. Schleicher U, Bogdan C. 2009. Generation, culture and flow-cytometric characterization of primary mouse macrophages. *Methods Mol Biol* 531:203–224. https://doi.org/10.1007/978-1-59745-396-7_14.
 83. Brandau S, Dresel A, Clos J. 1995. High constitutive levels of heat-shock proteins in human-pathogenic parasites of the genus *Leishmania*. *Biochem J* 310:225–232. <https://doi.org/10.1042/bj3100225>.
 84. Schneider CA, Rasband WS, Eliceiri KW. 2012. NIH Image to ImageJ: 25 years of image analysis. *Nat Methods* 9:671–675. <https://doi.org/10.1038/nmeth.2089>.
 85. Bogdan C, Stosiek N, Fuchs H, Röllinghoff M, Solbach W. 1990. Detection of potentially diagnostic leishmanial antigens by Western blot analysis of sera from patients with kala-azar or multilesional cutaneous leishmaniasis. *J Infect Dis* 162:1417–1418. <https://doi.org/10.1093/infdis/162.6.1417>.
 86. Thompson JD, Higgins DG, Gibson TJ. 1994. CLUSTAL W: improving the sensitivity of progressive multiple sequence alignment through sequence weighting, position-specific gap penalties and weight matrix choice. *Nucleic Acids Res* 22:4673–4680. <https://doi.org/10.1093/nar/22.22.4673>.